Reconstruction of palaeoenvironmental conditions of the Vaca Muerta formation in the southern part of the Neuquén Basin (Tithonian-Valanginian): Evidences of initial short-lived development of anoxia

Nesma Krim, Nicolas Tribovillard, Armelle Riboulleau, Viviane Bout-Roumazeilles, Cédric Bonnel, Patrice Imbert, Charles Aubourg, Guilhem Hoareau, Bertrand Fasentieux

Revised Version, Janvier 2019

Reconstruction of palaeoenvironmental conditions of the Vaca Muerta Formation in the Southern part of the Neuquén Basin (Tithonian-Valanginian): evidences of initial short-lived development of anoxia

Nesma KRIM[(1, 2,*)], Nicolas TRIBOVILLARD[(3)], Armelle RIBOULLEAU[(3)], Viviane BOUT-ROUMAZEILLES[(3)], Cedric BONNEL[(2)], Patrice IMBERT [(1)], Charles AUBOURG[(2)], Guilhem HOAREAU[(2)], Bertrand FASENTIEUX[(2)]

[(1)] CSTJF, TOTAL, S.A. Avenue Larribau. 64018 Pau Cedex, France

[(2)] Université de Pau et des Pays de l'Adour, Laboratoire des Fluides Complexes et de leurs Réservoirs, UMR CNRS TOTAL 5150. Bâtiment IPRA, BP1115, 64013 Pau cedex, France

[(3)] Université de Lille , Laboratoire LOG, UMR 8187 CNRS-ULille-ULCO, bâtiment SN5. 59655 Villeneuve d'Ascq Cedex, France

[(*)] Corresponding author: nesma.krim@gmail.fr

Abstract

The Vaca Muerta Formation is a famous source rock being largely present in Argentina. The formation was examined in the southern part of the Neuquén Basin through clay-mineral assemblage composition, as well as organic and inorganic geochemical characteristics. In total, 259 samples were analyzed on both sides of the Huincul Arch (major E-W structure that divided the southern part of the basin into two depocentres). South to this structure (Picún Leufú area), the total organic carbon content (TOC) can reach 20% but is generally ranging from 0.1 to 6%. To the north (Covunco area), average TOC does not exceed 0.5%. Clay-mineral assemblages indicate an evolution of the sources of clastic supply through time in response to evolving weathering/erosion at the regional scale. Redox-sensitive trace-element distribution shows that the particulate iron shuttle process operated, with an initially-euxinic depositional environment that evolved rapidly to oxygenated seawater and suboxic sediments. Our results suggest an episodically restricted circulation pattern that occurred at the beginning of the deposition of the Vaca Muerta Formation (highest TOC content).

Keywords: Neuquén Basin, Vaca Muerta Formation, Source rocks, Clay mineralogy, Trace elements, Paleoenvironmental evolution, Particulate shuttle effect.

1. Introduction

The Vaca Muerta Formation is one of the most prolific source-rocks of the Neuquén Basin (Argentina). It is known for its shale-gas potential with an average total organic carbon (TOC) locally exceeding 4%, moderate burial depth (≈ 2400 m) and over-pressured conditions (Boyer et al., 2011; Giusiano et al., 2011). This lithostratigraphic unit consists of dark shales, marls and limestones deposited during the Tithonian-Valanginian interval, as the result of a rapid and widespread marine transgression (Legarreta and Uliana, 1991, 1996b). Several previous works interpreted the Vaca Muerta Formation to be made up with both basin and slope deposits (e.g., Weaver (1931), Groeber (1946, 1953), Marchese (1971), Leanza (1973), Leanza et al. (1977), Gulisano et al. (1984), Mitchum and Uliana (1985), and Legarreta and Gulisano (1989)). Recently, detailed sedimentological studies were conducted in different sectors of the basin. Kietzmann et al. (2014) interpreted the Vaca Muerta Formation in the Mendoza area as a result of a double carbonate-ramp configuration: the first one corresponded to a westward progradation of a homoclinal ramp located on the eastern margin, and the second one corresponded to the outermost part of a distally-steepened ramp located in the present-day Chilean territory. In the southern part of the basin (Picún Leufú Anticline), Krim et al. (2017) interpret the Vaca Muerta Formation as a prograding siliciclastic shelf with storm and turbidity flows, and with an episodic, moderate, limitation of marine circulation, at least during the beginning of the Vaca Muerta deposition. Based on field observations (several sections), microfacies analysis, mineralogical and geochemical analyses of a limited sample set (one section), these authors observed that the Vaca Muerta Formation did not record oxygen-limited conditions, contrary to expectation, except for the very base of the formation. In addition, the organic content of the rocks is rather poor, again except for the basal level of the formation that seems to have undergone peculiar conditions of deposition (euxinic environment prone to organic matter preservation and accumulation).

In this paper, we present an extended and detailed mineralogical and geochemical examination of the Vaca Muerta Formation in the southern part of the Neuquén Basin (Picún Leufú Anticline) studying notably the clay-mineral assemblages and the major- and trace-element distributions, in addition to Rock Eval Pyrolysis data. Our goal is to examine the redox status of the southern part of the Neuquén Basin during the Vaca Muerta Formation deposition, in complement to what is already well known for the more distal parts of the basin, to the North (Kietzmann et al., 2014, and references therein). Were the more proximal

parts of the basin undergoing reducing conditions? What was the productivity like during the Vaca Muerta deposition? Which were the main sources of organic matter and clastic supply? How did these parameters evolve through time in possible relation with varying climatic conditions and on-land physiography? We also aimed to study the basal level of the formation that seems to be very specific and to be a regional marker level. Our replies to these questions are of course typically relevant for the Vaca Muerta Formation, which is a major source rock as well as an excellent case study yielding rich information one can apply to many other source rocks of any age in many other basins through the world. Our results may be of interest to petroleum geologists and "paleo-environmentalists".

2. Geological setting

2.1. Regional geology

The Neuquén Basin (Figure 1-A) is located between 32°S and 41°S in latitude and covers an area of over 120,000 km^2 (Yrigoyen, 1991). It has a triangular shape and is limited by the Sierra Pintada Massif to the northeast, the Patagonian Massif to the south and the Andean Arc to the west (Howell et al., 2005). It was formed in a back-arc extensional setting during the early stages of the Andean Orogeny (Digregorio and Uliana, 1980).

The basin was initiated during the Late Triassic by the extensional collapse of the Late Paleozoic orogen. This phase allowed the development of a series of narrow and isolated half-grabens, filled with continental and volcanic red-bed facies (Manceda and Figueroa, 1995; Vergani et al., 1995; Franzese and Spalletti, 2001). From the Early Jurassic to the Early Cretaceous, the Neuquén Basin was a back-arc basin, associated with the subduction of the proto-Pacific crust beneath the western Gondwana margin (Vergani et al., 1995). The protracted period of thermal subsidence and regional back-arc extension (Howell et al., 2005) allowed the development of a marine basin that was connected to the proto-Pacific Ocean by gaps in the arc (Spalletti et al., 2000; Macdonald et al., 2003). A complex series of transgressive-regressive cycles developed during this period as a result of subsidence rate variations, eustatic sea-level fluctuations and localized uplifts (Figure 2; Gulisano et al., 1984; Legarreta and Gulisano, 1989; Legarreta and Uliana, 1991, 1996 a, b). The regime of regional thermal subsidence was interrupted by several episodes of structural inversion (Vergani et al., 1995; Veiga et al., 2001; Pángaro et al., 2002). These tectonic inversions caused or enhanced relative sea-level falls and resulted in the accumulation of six wedges that sharply overlie deep-marine deposits. From the Late Cretaceous to the Cenozoic, the basin was characterized

by a compressional tectonic regime associated with a decrease in the angle of slab subduction that produced the uplift of the foreland thrust belt (Ramos, 1999b). Flexural subsidence towards the east of the tectonic front allowed for the accumulation of over 2000 m of continental syn-orogenic deposits (Legarreta and Uliana, 1991; Ramos, 1999b).

2.2. Local geology

The analyzed time interval of the present paper is the Tithonian-Berriasian (Figure 3). In the southern part of the Neuquen basin, sedimentary rocks deposited during this time interval comprised two marine lithostratigraphic units known as the Vaca Muerta and Picún Leufú formations (Leanza, 1973). The Vaca Muerta Formation (locally dated of early to earliest-late Tithonian) consists of a thick succession of dark bituminous shales and marls whereas the Picún Leufú Formation consists of mixed carbonate and siliciclastic sediments (Armella et al., 2007; Spalletti et al., 2000). Spalletti et al. (2000) interpreted the Tithonian-early Berriasian succession of this part of the Basin (Vaca Muerta-Picún Leufú formations) as deposited on a gently sloping marine ramp (mixed siliciclastic-carbonate deposits) with a gradual transition from a shallow marine area along the southern and southwestern margins of the basin, to the deepest area to the north. In a recent study (Krim et al., 2017), two transgressive-regressive sequences were recognized in this time interval and interpreted as developed in a siliciclastic shelf evolving to mixed siliciclastic-carbonate ramp.

During the late Oxfordian to Kimmeridgian times, an important tectonic inversion related to a change in the subduction regime along the active margin of the basin (Vergani et al., 1995) occurred in this part of the basin. The uplift of the Huincul Arch then divided the wide embayment of the Neuquén Basin into two main sedimentary depocentres (Zavala et al., 2005; Mosquera and Ramos, 2006) (Figure 1-B). The Huincul Arch represented a structural and stratigraphic barrier that isolated the southern depocentre. Thickness analysis of the Tordillo Formation suggests the existence of two depocentres in the northern part of the basin (Vergani et al., 1995; Spalletti and Colombo Pinol, 2005). In the southern part of the basin, the Kimmeridgian sediments correspond to <40 m-thick fluvial deposits of the Tordillo Formation (Groeber, 1946) grading to the eolian deposits of Quebrada Del Sapo Formation (Digregrio, 1972. This information suggests a structural activity of the Huincul Arch before the Tithonian whereas a recent study (Massaferro et al., 2014) indicates that the tectonic activity of the Huincul Arch was initiated during the Late Berriasian with a maximum activity during the Early Valanginian.

To the north of the Huincul Arch, the Vaca Muerta Formation has been divided into three members: (1) the Lower Vaca Muerta Member consists of bituminous shales and marlstones, (2) the Los Catutos Member consists of lithographic limestones and (3) the overlying Upper Vaca Muerta Member consists of siltstones, shales and marlstones (Figure 3; Leanza and Zeiss, 1990).

The east-west oriented Picún Leufú Anticline (the main study area in this paper) defines the western portion of the Huincul Arch and constitutes the main paleo-topographic feature of the region (Naipauer et al., 2012) which isolated the southern depocentre (Figure 1-B). The Covunco area locality (the second study area in this paper) corresponds to the SE part of the Sierra Vaca Muerta Anticline and thus to the south part of the western depocentre (Figure 1-B). In this part of the basin, the Tithonian–Berriasian interval corresponds to the Lower Vaca Muerta Member, the Los Catutos member, the Upper Vaca Muerta Member and Picún Leufú Formation (Leanza, 1973; Leanza and Zeiss, 1990).

3. Samples and methods

Rock samples were collected on two spots in the southern part of the Neuquén Basin. The first study area is located on the north flank of the Picún Leufú Anticline, south to the town of Zapala; the second spot is the Covunco section (north of Zapala Town; Figure 1).

In this study, 259 samples were collected from outcrops. 221 samples were collected in the Picún Leufú area and most of them cover the Vaca Muerta Formation (Major T-R sequence I). Only section 3 and two samples of section 5 (#41 and #42) extend to the major sequence II (Picún Leufú Formation). Samples were taken with an average spacing of 1-1.5 m in the basal sixteen meters (section 1, 4 and 5) of the study interval to analyze in detail the black shales and other samples were taken along the section, with irregular spacing to have the overall evolution of the study interval. 38 samples were collected in Covunco area, covering the Lower Vaca Muerta Member, the Los Catutos member and a part of the Upper Vaca Muerta Member.

The carbonate content was determined with a Bernard-type calcimeter (acid digestion followed by CO_2 volume determination; accuracy < 5%). The clay fraction was isolated and analyzed using the standard protocol for determining clay-mineral assemblages (using a Bruker D4 Endeavour XRD system together with the Macdiff software; see detailed protocol in Bout-Roumazeilles et al., 1999). The major- and trace-element contents were analyzed by

ICP-OES and ICP-MS at the spectrochemical laboratory (SARM) of the Centre de Recherches en Pétrographie et Géochimie of Vandœuvre-les-Nancy (geochemistry laboratory of the French Centre National de la Recherche Scientifique - CNRS). The samples were prepared by fusion with $LiBO_2$ followed by HNO_3 dissolution. Precision and accuracy were both better than 1% (mean 0.5%) for major-minor elements and 5% for trace elements, as checked by international standards and analysis of replicate samples (Carignan et al., 2001). Enrichment factors (EF) were calculated as: $XEF = [(X/Al)_{sample}/(X/Al)_{PAAS}]$, where X and Al represent the weight % concentrations of element X and Al, respectively. Samples were normalized using the post-Archean average shale (PAAS) compositions of Taylor and McLennan (1985). In most frequent procedures, aluminum normalization is commonly used to minimize the effects of variable dilution by carbonate or biogenic silica, although certain caveats apply to this approach (for a discussion as well as the rationale we used to interpret trace-element data, see Tribovillard et al., 2006 and Van der Weijden, 2002). Calculating enrichment factors allows us comparing the trace element abundance of the studied rocks with that of a reference of the wholesale clastic supply, namely the average Earth's upper crust composition (McLennan, 2001) or the PAAS (Taylor and McLennan, 1985). Any enrichment-factor value greater than 1.0 corresponds to the enrichment of an element relative to its average crustal abundance. In practical terms, EFs >3 represent the detectable enrichment of an element over its average crustal concentrations, and EFs >10 represent a moderate to extreme enrichment (Algeo and Tribovillard, 2009). Detailed results are given in Appendix 1.

Interpretations of the abundances of the redox-sensitive trace metals and/or productivity-proxying elements are based on the general considerations recently published (Brumsack, 2006; Tribovillard et al., 2006; Algeo and Rowe, 2012; and references therein).

Organic matter was analyzed using Rock Eval 6 pyrolysis on outcrop samples of the two study areas. Rock-Eval pyrolysis is used to evaluate kerogen type, quality and maturity of source rocks (Espitalié et al., 1985; Lafargue et al., 1998). For this paper, the following parameters were taken into consideration: total organic carbon, or TOC, expressed in weight %, Hydrogen Index (HI, in mg hydrocarbon per g TOC), Oxygen Index (OI, in mg CO_2 per g TOC) and Tmax (in °C). Detailed results are given in Appendix 2.

4. Results

4.1. Profile description

The study area corresponds to the east-west oriented Picún Leufú Anticline which defines the western portion of the Huincul Arch and constitutes the main paleo-topographic feature of the region (Naipauer et al., 2012) that isolated the southern depocentre (Figure 1-B). In the Picún Leufú zone, the Tithonian–Berriasian interval corresponds to two marine lithostratigraphic units known as the Vaca Muerta and Picún Leufú Formations (Figure 3; Leanza, 1973).

Sedimentological log sections of the Picún Leufú Anticline are taken from Krim et al. (2017), (Figure 4) where detailed descriptions of the lithofacies and stratigraphy are given. Only a summary is presented here. The study interval is of the Tithonian-Berrisian in age and consists of two major transgressive-regressive sequences (*sensu* Embry and Johannessen, 1992) that correspond to siliciclastic shelf system (according to the nomenclature of Walker and Plint, 1992) (Major T-R sequence I, Vaca Muerta Formation) evolving to a mixed siliciclastic-carbonate ramp (according to the nomenclature of Burchette and Wright, 1992) (Major T-R sequence II, Picún Leufú Formation). The siliciclastic shelf exposes mainly (1) fine grained sediments corresponding to grey silty shales deposited in an offshore environment, affected by storm and gravity currents, and (2) storm beds and slumps in the offshore-shoreface transitional zone, and (3) sandstones attributed to a lower shoreface setting. The mixed siliciclastic-carbonate ramp environment displays (1) green silty shales attributed to the outer ramp, (2) storm beds in the middle ramp and (3) development of tidal deposits, shoal facies and lagoonal carbonates in the inner ramp.

The Covunco area locality corresponds to the SE part of the Sierra Vaca Muerta Anticline and thus to the south part of the western depocentre (Figure 1-B). In this part of the basin, the Tithonian–Berriasian interval corresponds to the Lower Vaca Muerta Member, the Los Catutos member, the Upper Vaca Muerta Member and Picún Leufú Formation (Leanza, 1973; Leanza and Zeiss, 1990).

According to the ammonite biozones (Leanza and Zeiss, 1990, 1992), the sampled interval is also of Tithonian age. It corresponds to a siliciclastic shelf (according to the nomenclature of Walker and Plint, 1992) that evolves to a mixed siliciclastic-carbonate ramp (according to the nomenclature of Burchette and Wright, 1992). The siliciclastic shelf exposes mainly (1) fine grained sediments corresponding to grey silty shales deposited in an offshore environment, affected by storm and gravity currents and (2) storm beds with HCS in the offshore-shoreface transitional zone. The mixed siliciclastic-carbonate ramp environment displays two main zonations corresponding to (1) the outer ramp that exposes grey marls with rare

packstones/grainstones and (2) the inner ramp that exposes massive grainstones/packstones limestone beds with marls and evidence of tidal currents.

4.2. Mineralogy

The clay-mineral assemblages of the Picún Leufú area, analyzed on five sections (sections 1 to 5), are composed of smectite, illite, kaolinite, chlorite and mixed-layers (Figure 5). The proportions given below refer to the percentages within the clay mineral assemblages and not within bulk rock.

Smectite is the main clay mineral in this area. Its average proportion is around 70% and only a few samples show a low proportion in section 1 (samples #26 = 23% and #33 = 18%) and section 3 (samples #1 = 3% and #2 = 5%). Illite is always present except for sample #2 of section 3 and two samples of section 4 (samples #21, #35, #39). The average content is around 7% but a few samples are enriched in illite (section 1: samples #11 = 24%, #26 = 26%, #45 = 18%; section 2: sample #10 = 21% section 4: samples #3bis = 21%, #18 = 19%, #22 = 24 %).

Mixed-layers correspond here to illite-smectite mixed-layers (10-14S) in all the sections, except for one sample (section 2, sample #3) which shows a low proportion of chlorite-smectite mixed-layer 14C-14S (4%). The 10-14S mixed-layer content shows an overall residual distribution (< 5%) but can reach 22% in section 2 (sample #10). Section 3 shows two samples with high 10-14S mixed layer proportion (sample #50 = 47% and sample #52= 40%). They are located in the upper part of the section. In this area, kaolinite shows an erratic distribution. In sections 1 and 4, this clay mineral does not show any trend whereas an overall decreasing to the top is observed in sections 2, 3 and 5. Sections 1 and 4 record two major peaks of kaolinite at the middle of the sections (samples #26 =29% and #18= 28% , respectively) but the average value is globally low (5%) except for some samples where this clay mineral is more abundant (around 15%). Sections 2, 3 and 5 show two major peaks of kaolinite at the bottom of the sections (33%, 94% and 39%, respectively) but the average value is globally low (< 5%) except for some samples (between 8 and 13%). Section 3 is the richest in kaolinite. The average value is around 16% and several samples exceed 30% (sample #3= 37%, sample #4= 31, sample #5= 43%, sample #6= 38%, sample #7= 45%, sample #9= 57%, sample #16= 43%, sample #22= 52%, sample #24= 56%). Figure 5 shows an overall decreasing trend of kaolinite proportions during the Late Jurassic. Chlorite is globally residual (< 5%) except in some samples where this clay mineral is more abundant (8-

12%) and can reach 22% (section 3, sample #17). In section 3, the upper part of the section (Major T-R sequence II), this clay mineral reaches 30% of the clay mineral fraction (sample #43).

The nature of clay-mineral assemblages of the Covunco area is similar to the other sections, being mainly composed of smectite, kaolinite and illite (Figure 5). It displays a less-distinct smectite-dominated trend than the first study area. Smectite content is distributed on two contrasting intervals: first, low values in the lower part of the section (from sample #1 to sample #10) except for sample #2 (89%), then an erratic distribution with an overall increasing up to the top of the section (samples #14, #15, #17, #23, #24, #27, #28, #30, #32, #37 show low smectite content). Illite is always present except for samples # 2, 11, 16. It shows high values in the lower part of the section (from sample #1 to sample #10, except for the sample #2), then an overall decreasing to the top of the section with an erratic distribution. Kaolinite distribution shows a major shift above the three basal samples, jumping from <15% to >45% but this concentration rapidly decreases upward yielding residual content with scarce peaks (from sample #16 to sample #38). 10-14S mixed-layers show an erratic distribution and are mainly present in the lower part of the section (samples # 3 to # 15). The upper part or the section shows two peaks around sample #23 (= 13%) and #24 (= 14%). Chlorite is globally residual (< 15%) except for the bottom of the section (sample # 1, with 58%).

In summary, the average clay composition of sections 1 to 5 is very similar (Table 1, Figure 6), being enriched in smectite. The Covunco section displays a very different average composition, showing higher contribution of illite and chlorite, whereas kaolinite contribution is somehow similar to what is observed for the other sections. The variability is also higher in the Covunco section.

In a ternary diagram, showing a distribution between primary clay minerals (i.e. little or not altered, represented by chlorite+illite), weathered clay (kaolinite), and mixed layers (smectite +IS), all sections show a distribution close to the S+IS end-member (Figure 7). Nevertheless sections 1 and 4 show high scattering towards the illite+chlorite and the kaolinite end-members, respectively. Samples of section 2 are more centered on the S+IS end-member and only display a slight scattering toward both the kaolinite and the illite+chlorite end-members. The basal sample is also enriched in kaolinite (Figure 7). Samples of section 3 show high scattering between the S+IS and the kaolinite end-members. Samples enriched in kaolinite correspond to samples collected in the lower part of the section. In section 5, all samples plot

very near to the S+IS end-member showing very little linear scattering toward the primary clay end-member, except for sample#1 which is characterized by its high content in kaolinite (Figure 7).

The Covunco series display a distinct pattern, being distributed between the S+IS and primary clay end-members, with a variable contribution of kaolinite (Figure 7).

These observations suggest the existence of a S+IS-rich source which largely fed the deposits of the section 5 with some minor contribution of I+C. This source also dominates in section 2 in association with some contribution of a kaolinite-rich source. The contribution of the I+C source is higher in section 1, while the contribution of the kaolinite-rich source increases in section 4 and is at its maximum in section 3.

The Covunco series appears as much more influenced by the primary clay-rich source.

4.3. Geochemistry

The chemical index of alteration or CIA reflects the degree of transformation by weathering of alumino-silicate minerals (Nesbitt, 2003): CIA = 100 × Al_2O_3 / (Al_2O_3 + Na_2O + K_2O + CaO*), where the calculation is molar based, and CaO* represents the CaO content corrected for carbonate. Primary minerals (little or not altered) have a CIA about 50 or less, whereas secondary clay minerals have CIA values of 75 or more. The CIA is a quantitative estimation of the amount of chemically weathered materials included in a siliciclastic sediment or rock, and reflects chemical weathering intensity on source lands (Nesbitt, 2003). The CIA values of the Picún Leufú and Covunco areas range from 45 to 75 (Figure 8). The comparison of the CIA index and the chlorite/kaolinite (C/K) ratio, where chlorite is a primary clay while kaolinite is a weathered clay (Figure 8), shows very few levels where both indicators are in agreement (blue rectangles on Figure 8).

4.4. Trace metals

4.4.1. Redox proxies

Regarding uranium (U) and molybdenum (Mo), throughout all the sample sets studied here, none of them two is correlated to aluminum, which indicates that these elements are not of dominant terrigenous origin in the basin. The five sections of the south part of the basin (1 to 5) show a similar pattern with a pronounced enrichment in Mo (up to 200 x average crustal abundance in some occurrences) but a generally limited U enrichment (EF>5; Figure 9). All

these samples fall into the part of the U-EF vs. Mo-EF diagram that corresponds to the particulate iron shuttle process, as defined by Algeo and Tribovillard (2009). Only a limited number of samples show enrichment in both elements (Figure 9), they correspond to the basal level of the sections. Contrastingly, the Covunco section sample set shows a different distribution, with the same order of Mo enrichment as that of the other sections, but a higher U enrichment. These samples fall into the part of the U-EF vs. Mo-EF diagram that corresponds to the suboxic to anoxic trend (Figure 9).

Regarding vanadium (V), for the six sections studied, the enrichment factor generally keeps at low values. For the southern five sections, only the basal samples showing relatively high U and Mo concentrations also show moderate enrichment in V. For the Covunco section, V concentration is well correlated to Al contents (terrigenous, clastic origin), except for the few samples with the highest V, Mo and U concentrations (Appendix 1).

A peculiar aspect is that arsenic (As) and antimony (Sb) both show appreciable enrichment throughout the studied sample sets. Both As and Sb show mutual correlation and significant correlations to Mo (Appendix 1).

In several sections the basal samples are singular in that they may show high to very high enrichments in several trace metals (As, Mo, Pb and Zn) and noticeable enrichments in U and Sb (Appendix 1).

4.4.2. Productivity proxies

For the six sections of interest, the elements considered to be robust proxies to paleoproductivity (namely, Ba, Ni and Cu; e.g., Brumsack, 2006; Tribovillard et al., 2006; Böning et al., 2012; Böning et al., 2015 and references therein) do not show marked enrichment, even for the basal samples evoked above (some of the latter samples show only a detectable, yet faint enrichment, Appendix 1). The role of Ba as a paleoproductivity tracer is questionable here: the element is commonly used as a proxy for marine setting with a thick water column, and it is not sure in the present case, whether the water column was thick enough for Ba to be significantly trapped into settling bioparticles.

4.5. Organic matter

In the Picún Leufú area, the TOC values of the Vaca Muerta Formation range from 0.01% to 24.5%. Despite some variability, a similar vertical trend of TOC values is observed in

sections 1, 3, 4 and 5 (Figure 10). A maximum of more than 20% TOC is observed in the lowermost sample (sections 1, 3 and 5), followed by a rapid drop to values generally lower than 6%. These high TOC values are maintained in the lower 100 to 150 m of the sections. Above 150 m, the TOC values are generally below 1.5%. Section 2 contrasts with this trend and shows very low TOC values, in particular in the lower part of the section (Figure 10). Maximum values up to 1.7% are observed in the middle part of the analyzed interval. Very low TOC values (<0.2%) are observed in the Picún Leufú Formation. In the Covunco area, TOC values are low compared to Picún Leufú area (Figure 10), ranging from 0.1% to 3.3% with an average value around 0.2%. The highest value is recorded in the lower part of the section (sample #14).

Because of their low organic matter content, a number of samples (111 out of 259) showed a low S2 peak intensity, preventing the safe interpretation of T_{max} values. Nevertheless, considering the appropriate samples allowing for paleoenvironmental reconstructions, we may say that the the Picún Leufú Formation shows Tmax values indicating a low maturity stage. The samples that are not suitable with regards to Tmax values also show anomalously high OI values pointing to (postdepositional?) oxidation/alteration of the organic matter (Espitalié et al., 1985). These samples are particularly present in the upper part of section 3 (Picún Leufú Formation), in section 2 and in Covunco (strong burial diagenesis). These values were not taken into consideration in what follows.

Hydrogen index values range between 15 and 644 mg HC/g TOC (Figure 10). In Picún Leufú area, the vertical evolution of HI values is parallel to that of TOC values, with values above 300 mg HC/gTOC observed in the lower 150m of the sections, and values lower than 200 mg HC/gTOC in the upper part. Apart from sample #24, low HI values are observed in section 2. In the Covunco area, HI values are low, except for a few samples in the lower part of the section (Figure 10).

Oxygen index values range between 11 and 436 mg CO_2/g TOC, with an average value of 117 in Picún Leufú area and 205 in Covunco area. No clear vertical trend of OI values is observed though low values are more common in the lower part of sections in the Picún Leufú area (not shown). Using a pseudo-Van Krevelen diagram (Hydrogen Index versus Oxygen Index plot, Figure 11-A),the data plot in the kerogen Types II, III and IV. A positive correlation between HI and TOC values is observed for all samples (Figure 12-A), indicating that Type II kerogen predominates in samples with a high content in organic matter, while

kerogen Type III to IV predominates in samples with a low organic content. The correlation between HI and TOC values in Covunco area is shifted to lower TOC values and/or higher HI values, compared to Picún Leufú area (Figure 12-A)

T_{max} values range between 409 and 444°C with a mean value of 426°C in the Picún Leufú Anticline and 437°C in the Covunco area (Figure 11-B). A general positive correlation is observed between IO and Tmax values (r=0.68, Figure 12-B); nevertheless, samples from Covunco show a correlation shifted toward higher Tmax values, compared to Picún Leufú area (Figure Y-B). This indicates that, despite an effect of oxidation on Tmax values, the organic matter is thermally immature in the Picún Leufú Anticline, while it is more mature (beginning of the oil window) in the Covunco area.

5. Interpretation/Discussion

5.1. Paleoclimatic evolution

The different clay-mineral distribution from the Picún Leufú area to the Covunco area and the progressive stratigraphic evolution in each analyzed spot can be the result of an evolution of the weathering conditions affecting emerged lands or a change in the sources of the sediments during the course of the deposition of the Tithonian/Valanginian sediments at stake here (Chamley, 1989). In both Picún Leufú and Covunco areas, the evolution from kaolinite-dominated to smectite-dominated situations can be the result of a climatic evolution toward less hydrolyzing conditions at the Jurassic-Cretaceous transition. The CIA distribution is globally more monotonous than the clay mineralogy in most samples and no interpretable trend or evolution is observed. The contrasting response of each proxy (clay mineral vs. CIA) suggests that the same process was recorded differently in the various mineralogical/grain size fractions of the sediment (clays vs. bulk sediment). In the present case, the clay-sized fraction of the sediments represents only a small part of the clastic fraction, compared to the silt fraction. Consequently, some variation may affect the clay-fraction without being clearly recorded by the CIA that would be more impacted by what occurred to the feldspars of the silt fraction.

Regarding the sequence-stratigraphy framework established by Krim et al. (2017), the clay-mineral distribution is not in phase with sea-level variations, suggesting that the evolution of the clay-mineral content is not a response to the sea-level fluctuations and can thus be considered as a climatic imprint. This observation was previously established by Krim et al.

(2017) for section #3 and is here confirmed for the different sections of the Picún Leufú anticline. As previously suggested (Krim et al., 2017), fluctuations in the sedimentary environments and siliciclastic/carbonate supply likely record the latitudinal migration of the climatic belts. Under warm temperate climatic conditions, which dominated during the deposition of the Vaca Muerta Formation, seasonal rainfall provoked chemical weathering and high runoff, and promoted hydrolyzing conditions prone to kaolinite formation as well as the transport of the erosion by-products towards the basin. This configuration favored the development of a siliciclastic supply. Less-hydrolyzing conditions dominated during the deposition of the Picún Leufú Formation, indicated by relatively low CIA values and absence of kaolinite; the reduced terrigenous supply allowed for the relative increase of carbonate concentration and favored the development of a mixed siliciclastic-carbonate setting. Most of the samples analyzed in this paper were collected in the first major sequence (except two samples of section 2 and 21 samples of section 3). The trend in the clay-mineral content also recorded in this interval suggests that the climatic evolution began in the first major T-R sequence.

In the Covunco area, by analogy with the Picún Leufú area, the clay mineral evolution, and in particular the decrease of the kaolinite content, is also interpreted as a climatic imprint. The comparison between the two studied locations reveals a more complex evolution in the Covunco area than in the Picún Leufú area, where the decrease of kaolinite is accompanied by the decrease of illite. Besides, the Covunco section shows the constant occurrence of chlorite whereas this mineral is only residual in the Picún Leufú area. The presence of chlorite is likely reflecting transportation patterns and/or a different sediment provenance compared with the other sections. The differences observed at the two locations suggest that contrasting evolution of the weathering conditions affected emerged lands on the opposite sides of the Huincul Arch.

Lastly, the clay-mineral dataset shows an overall trend of kaolinite with decreasing proportions during the Late Jurassic (Figure 5). If interpreted in term of paleoclimate control on clay minerals, this trend suggests aridity somewhat grew with time to some extent. Such a climatic trend is well known for the Jurassic-Cretaceous boundary and has been largely observed in (peri-)Tethyan sections, from France and UK to Tunisia and the Russian platform, based on clay minerals data, but on palynological data as well (e.g., Deconinck, 1993; Abbink et al., 2001; Ruffell et al., 2002; Schnyder et al., 2006; Grabowski et al., 2013, among others).

5.2. Organic source(s) and productivity

The Rock Eval data reveal that the organic matter of the studied samples, collected on outcrops, suffered from weathering. This is indicated by the abundance of samples with very low TOC and with OI values above 300 mg CO_2/g TOC (Espitalié et al., 1985). In particular, it can be noted that most samples in section 2 and approximately half of samples in Covunco section were severely affected by weathering. From this observation, the results from "unoxidized" samples must be considered with caution, keeping in mind that even slight oxidation results in a decrease of TOC values of the rock and an evolution of organic matter bulk chemistry towards that of Type III kerogen (Durand and Monin, 1980; Petsch et al. 2000). Nevertheless, and despite the slightly higher thermal maturity in Covunco area, the available data from the less oxidized samples allow discussing the source of organic matter.

The correlation between HI and TOC values (Figure 12-A) is frequently observed in sedimentary rocks deposited in marine settings (e.g. Tyson 1995; Boussafir and Lallier-Vergès, 1997). This correlation indicates that OM sedimentation fluctuated between two modes: one mode was prone to organic matter enrichment in the sediment, and the other was not. In the organic-rich samples of the studied interval, Type II kerogen characterized by HI values > 400 mg HC/g TOC is dominant (Figure 12-A). Type II organic matter mainly originates from the autochthonous marine production, dominated by planktonic algae and bacteria (Tissot and Welte, 1979; Tyson, 1995). In classical models, enrichment of the sediments in Type II organic matter is ascribed to increased surface productivity and/or to enhanced organic matter preservation associated to reducing conditions in the sediment (Tyson, 2005). In the organic-poor samples of the studied interval, Type III to Type IV kerogen is observed (Figure 12-A). In absence of palynofacies observation allowing to ascertain the source of the organic matter, this Type III-IV kerogen could correspond to degraded organic matter of marine origin, and/or to organic matter of continental origin (Tissot and Welte, 1979; Tyson, 1995). Considering the relatively proximal depositional setting in this part of the Neuquén Basin (Krim et al., 2017), both sources of organic matter are likely. The mixed contribution of marine and terrestrial organic matter is supported by a palynological study of the middle part of the Vaca Muerta Formation in the Picún Leufú area, where dinoflagellates (marine algae) and an abundance of pollen grains and spores were described (Quattrocchio and Sarjeant, 1992). Classical models indicate that deposition of low

quantities of altered marine and/or continental organic matter is observed when marine productivity is reduced and/or when conditions are more oxygenated in the sediment, leading to the low preservation of the less recalcitrant marine organic matter (Tyson, 1995; Boussafir and Lallier-Vergès, 1997). The absence of enrichment of productivity proxies (Ba, Ni and Cu) in the studied samples (§ 4.4.2, Appendix 1) suggests that marine productivity remained modest during deposition of the Vaca Muerta and Picún Leufú Formations in this area of the Neuquén basin, implying that changes in organic matter deposition and enrichment might be related to fluctuations of redox conditions, as discussed below.

5.3. Redox conditions

The salient feature is that, among the six sections studied, the Covunco section is the only one showing a co-enrichment in U and Mo that indicates oxygen-limited conditions of deposition. The generally higher HI values in non-oxidized samples from Covunco area (Figure 12-A), suggesting better preservation of the organic matter, are consistent with more reducing conditions in this part of the basin.

The five sections representing the southern part of the Neuquén Basin, for their part, recorded the so-called particulate iron shuttle process (see the following papers for details about the particulate shuttle process: Crusius et al., 1996; Algeo and Lyons, 2006; Chappaz et al., 2008; Goldberg et al., 2009; Dellwig et al., 2010; Owens et al., 2012; Scott and Lyons, 2012; Scholz et al., 2013; Jilbert and Slomp, 2013). In a few words, the oxy-hydroxides of Fe (and Mn) that form particles in the oxidizing part of the water column easily bind to dissolved chemical species present in seawater, and incorporate them in a reversible way. During settling, Fe- and Mn-oxyhydroxides can thus adsorb significant amounts of Mo (Crusius et al., 1996; Chappaz et al., 2008; Algeo and Tribovillard, 2009; Helz et al., 2011; Kashiwabara et al., 2011; Martin et al., 2013; Little et al., 2015). The oxyhydroxides in turn bind to settling particles or flocs of OM, or stick onto clay minerals. Once deposited, they can be chemically reduced and thus release the ions they scavenged. These released ions can in turn get solubilized at the sediment-water interface or into pore waters. In the latter case, they can be engaged into diagenetic mineral phases (sulfides, carbonates, silicates, etc.). This process does not operate for U, and the contrasting behaviors of U and Mo allowed Algeo and Tribovillard (2009) to define a U-EF versus Mo-EF crossplot helping reconstructing paleoredox conditions (Figure 9).

In the present case, it means that the samples of the southern five sections studied in the present study collected Mo that was scavenged by Fe- (and probably Mn-) oxyhydroxides in an oxic water column. After deposition, Mo was released to pore water through reductive dissolution of the oxy-hydroxides, but Mo was kept trapped in the sediments by incorporation (sensu lato) on or into iron sulfides (e.g., pyrite). Thus, the sediments are enriched in Mo, but not (or hardly) in U, because the latter element is not sensitive to the particulate shuttle effect. This interpretation is reinforced by the absence of marked enrichment in V, which also indicates that bottom water conditions were not reducing. However, even if the water column was oxic, the fact that Mo was kept within the sediments indicates that reducing conditions developed at shallow depth below the sediment-water interface; otherwise, Mo would have escaped back to the water column together with pore waters during incipient sediment compaction.

Through the various sections studied, the samples rich in Mo also show enrichments in As and Sb. A co-enrichment in Mo, As and Sb associated to a particulate shuttle has already been observed (Tribovillard et al., 2013, 2015). The enrichment in Mo can clearly be attributed to the role of iron (and manganese) oxy-hydroxides through particulate shuttle processes, as detailed in Algeo and Tribovillard (2009), Helz et al. (2011), Scholz et al. (2011, 2013), and Scott and Lyons (2012). The relationship between Mo and As can be attributed to the same phenomenon, because the role of iron oxy-hydroxides in the transfer of As from the water column to the sediments has been well explored (O'Day, 2006; Vaughan, 2006; Berner et al., 2013; Sullivan and Aller, 1996; Minami and Kato, 1997; Cutter et al., 2001; Chaillou et al., 2003; Breier et al., 2012; Neumann et al., 2013). The same is true for antimony, because Sb and As are considered to have similar geochemical properties in marine and also river systems (e.g., Cutter et al., 2001; Asaoka et al., 2012).

In total, we can consider that Mo, As and Sb have been brought to the sediments together with iron oxy-hydroxides. During diagenesis, the trace metals must have been released from oxy-hydroxides and incorporated into pyrite, taking into account the high degree of trace-metal pyritization known for Mo, As and Sb (Huerta-Diaz and Morse, 1992; Bostick and Fendorf, 2003; Couture et al., 2010; Berner et al., 2013).

The shuttle process is already known to favor Mo enrichment (Dale et al., 2012; Berelson et al., 2013), but from the present study, we conclude that the shuttle process may also cause some enrichment in As and Sb. Such a co-enrichment in Mo, As and Sb was already observed

in some particular settings: cold hydrocarbon seepages in Southeastern France (Jurassic Terres Noires Formation; Tribovillard et al., 2013) and in the pockmark field of the Congo Fan and Gulf of Mexico (Hu et al., 2014; see also Bayon et al., 2011). However, caution must be taken, because syngenetic pyrite (i.e., formed directly in the water column of euxinic environments) may also incorporate Mo, As and Sb present in seawater (Berner et al., 2013). However, in the latter case, the development of euxinic conditions induces pronounced enrichments in Mo and U, in particular. Consequently, to conclude that Mo, P, As and Sb are enriched via the iron shuttle process, U concentrations cannot be markedly enriched.

The basal samples of a few sections with marked enrichment in TOC and redox-sensitive trace metals, but no enrichment in productivity proxies (Ba, Ni, Cu), reflect reducing, oxygen-deprived conditions of deposition, with no indication of strong productivity. Thus organic-matter preservation must be ascribed to the absence of dissolved oxygen (probable euxinic conditions) as echoed by the marked enrichments in redox-sensitive and/or sulfide-forming trace metals. Apart from these few samples corresponding to the basal ammonite-rich level, most samples having higher enrichment factors in Mo than in U, recorded the particulate iron shuttle and, therefore, experienced conditions of depositions under oxic waters and with reducing conditions developing at shallow depth below the sediment-water interface. The samples of the top part of the southern sections show no interpretable authigenic enrichment in trace metals, which suggests deposition under fully oxygenated seawater.

5.4. Deep-water restriction/renewal

In addition to the oxygenation level of the basin, the degree of deep-water restriction may also be assessed through Mo and TOC concentrations. The degree of deep-water restriction has the potential to influence authigenic U–Mo enrichment of marine sediments. Water-mass restriction will reduce resupply of aqueous, trace metal species from the global ocean resulting in limited transfer of trace metal to sediments, thence limited enrichments (Algeo and Lyons, 2006; Little et al., 2015). However, water mass restriction is often correlated with other environmental variables such as redox conditions, and more reducing conditions in a restricted basin (especially within the suboxic–anoxic redox range) may enhance trace metal uptake, which may restrain or exhaust the pool of redox-sensitive, dissolved trace elements. Such an exhaustion (even if partial) will lower the enrichment in redox-sensitive trace metals, and the reducing paleo-condition will be masked in the sediment record. Thus, assessments of the hydrographic, aqueous chemical, and redox conditions of a particular paleomarine system

are best undertaken using a combination of proxies and analytical approaches (Tribovillard et al., 2012; Little et al., 2015). Keeping in mind that some TOC values might be decreased by surface weathering, a TOC vs. Mo diagram (Algeo and Lyons, 2006; Algeo et al., 2007) has been designed to visualize the paleo-degree of water mass restriction (Figure 13). This diagram is based on the analysis of some well-known, present-day environments, being used as references (Figure 13). In such a TOC vs. Mo diagram, the main feature is a rather indistinct distribution for the samples of any section with TOC < 5% (Figure 13). However, we observe a dominant "Saanich Inlet-type" distribution for sections 3 and 4, suggesting moderate water mass restriction. Furthermore, the samples of section 3 with the highest TOC values straddle the areas of the diagram that reflect increasing restriction and dissolved-Mo drawdown. These samples suggest deposition under a somewhat more marked water-mass restriction. They are located in the bottom part of the section, which tends to indicate that the depositional environment underwent episodic limitation of water mass circulation during the deposition of the lower part of the Vaca Muerta Formation (Late Jurassic). The samples from sections 5 and 1 are distributed along a trend in-between the Framvaren Fjord and Black Sea pattern (Figure 13), suggesting a moderately restricted situation. Most samples from Covunco and section 2 plot on the vertical axis, suggesting the absence of any limitation of water-mass circulation during the period of time at stake here. However, as previously discussed, numerous samples from these two sections suffered intense organic matter weathering. The Mo-TOC plot therefore cannot confidently be used for these two sections.

To sum up, focusing on the less oxidized samples with significant TOC values, Mo concentrations vs. TOC values relationships indicate that the water masses may have been relatively confined during the lower part of the episode of deposition of the Vaca Muerta Formation. Such a confinement then vanished, as indicated by the absence of enrichment in redox-proxying trace metals, as mentioned in the previous section.

5.5. Organic matter and sequence stratigraphy

The overall distribution of organic matter (TOC values) in the study area shows a large vertical and lateral variation in the Vaca Muerta interval (major T-R sequence I) (Appendix 2). According to the sequence stratigraphy framework of the Picún Leufú Anticline (Krim et al., 2017), the high TOC values corresponds to the upper part of the transgressive system tract (TST) and the lower part of the regressive system tract (RST) (Figure 14). The highest TOC value (>20%) is located in the TST below the main MFS of the study interval. Enrichment in

organic matter is a result of three main factors: productivity, dilution and destruction (Bohacs et al., 2005; Tyson, 2005; Tribovillard et al., 2005; Passey et al., 2010). According to Bohacs et al. (2005) and Tribovillard et al. (2005), dilution is the main control in proximal areas whereas primary organic production is dominant in the distal areas. This configuration allows concentrating organic matter in the TST intervals in the proximal setting and in the RST in the distal setting. According to these authors, our data suggest that both dilution and production play a role. During increasing sea level, the Vaca Muerta was in "distal" configuration (sensu Bohacs et al., 2005) and organic production was the main factor that played a role in the organic matter accumulation. In contrast, the beginning of sea level fall initiated a "proximal" configuration (sensu Bohacs et al., 2005) and dilution was then the main control factor.

To sum up, the highest enrichments in organic matter during the TST are linked to enhanced paleoproductivity in a "distal" context, whereas lower TOC values observed during RST seems to be linked to dilution processes in a "proximal" context.

6. Conclusions

Our main results about the Vaca Muerta Formation in the southern part of the Neuquén Basin may be recapitulated as follows:

1 - The depositional environment evolved from early conditions propitious to a short-lived episode of euxinia, and (thence) organic matter storage in great proportions, that was recorded at various places, passing to conditions with oxygenated sea water and suboxic sediments (propitious to the particulate shuttle process, and fairly good organic-matter accumulation), and ending with oxygenated water masses and oxic sediments with poor organic content.

2 – The water masses must have kept oxygenated (with the exception of the basal level) but some moderate restriction of seawater circulation may have been recorded, with little impact on sediment geochemistry.

3 – According to trace-element proxies, productivity must have remained at a modest level, through the deposition of the Vaca Muerta Formation. Consequently, organic matter storage was rather governed by favoring factors linked to sedimentation rates (dilution) and redox conditions (suboxic sediments).

4 – The composition of the clay-mineral assemblages, coupled to inorganic geochemistry allowed us to observe a clear evolution of the weathering/erosion at the regional scale. In addition, our results indicate that the observed evolution of the climatic conditions affecting emerged lands had no detectable impact on the deposition conditions constraining organic matter accumulation in the Neuquén Basin.

Beyond the Vaca Muerta Formation itself, the present work further supports the idea that a co-enrichment in Mo, As and Sb with no marked enrichment in U and V, is the signature of the iron shuttle process. This result deserves further testing with other types of sediments and rocks. If confirmed, it would be applied widely as a means to identify past processes involving the particulate shuttle effect.

Acknowledgments

This paper is a part of the PhD studies of the first author, undertaken at the university of *Pau et des Pays de l'Adour* (France) and sponsored by *TOTAL S.A*. The authors thank *TOTAL S.A* for permission to publish this paper. The reviewers (and among them Dr. J. Schnyder) as well as the Editor in charge of the manuscript are warmly thanked because they helped us improve substantially our paper.

Raw data are available in the supplementary material file.

References

Abbink, O., Targarona, J., Brinkhuis, H., Visscher, H. 2001. Late Jurassic to earliest Cretaceous palaeoclimatic evolution of the southern North Sea. Global and Planetary Change, 30, p. 231-256.

Algeo, T.J., Lyons, T.W., 2006. Mo-total organic carbon covariation in modern anoxic marine environments: implication for analysis of paleoredox and –hydrographic conditions. Paleoceanography, 21, PA1016, doi: 10.1029/2004PA001112.

Algeo, T.J., Tribovillard, N., 2009. Environmental analysis of paleoceanographic systems based on molybdenum-uranium covariation. Chemical Geology, 268, 211-225.

Algeo, T.J., Rowe, H., 2012. Paleoceanographic applications of trace-metal concentration data. Chemical Geology, v. 324–325, p. 6–18.

Algeo, T.J., Lyons, W.L., Blakey, R.C., Over, D.J., 2007. Hydrographic conditions of the Devono-Carboniferous North American Seaway inferred from sedimentary Mo– TOC relationships. Palaeogeography, Palaeoclimatolology, Palaeoecolology. 256, 204–230.

Armella, C., Cabaleri, N., Leanza, H.A., 2007. Tidally dominated, rimmed-shelf facies of the Picún Leufú Formation (Jurassic/Cretaceous boundary) in southwest Gondwana, Neuquén Basin, Argentina. Cretaceous Research 28, 961-979.

Asaoka, S., Takahashi, Y., Araki, Y., Tanimizu, M., 2012. Comparison of antimony and arsenic behavior in an Ichinokawa river water-sediment system. Chemical Geology, 334, 1-8.

Bayon, G., Birot, D., Ruffine, L., Caprais, J.-C., Ponzevera, E., Bollinger, C., Donval, J.-P., Charlou, J.-L., Voisset, M., Grimaud, S., 2011. Evidence for intense REE scavenging at cold seeps from the Niger Delta margin. Earth and Planetary Science Letters, 312, 443-452.

Berelson, W.M., McManus, J., Severmann, S., Reimers, C.E., 2013. Benthic flux of oxygen and nutrients across Oregon/California shelf sediments. Continental Shelf Research, 55, 66-75.

Berner, Z.A., Puchelt, H., Nöltner, T., Kramar, U., 2013. Pyrite geochemistry in the Toarcian Posidonia Shale of south-west Germany: Evidence for contrasting trace-element patterns of diagenetic and syngenetic pyrites. Sedimentology, 60, 548–573.

Bohacs, K. M., Grawbowski, G. J., Carroll, A. R., Mankeiwitz, P. J., Miskell-Gerhardt, K. J., Schwalbach, J. R., Wegner, M. B., Simo, J. A, 2005. Production, Destruction, and Dilution – the Many Paths to Source-Rock Development, SEPM Special Publication 82, p. 61-101.

Böning, P., Brumsack H-J, Schnetger, B., Grunwald, M., 2009. Trace element signatures of Chilean upwelling sediments at ~36°S. Marine Geology 259, 112-121.

Böning, P., Shaw, T., Pahnke, K., Brumsack H-J, 2015. Nickel as indicator of fresh organic matter in upwelling sediments. Geochimica et Cosmochimica Acta 162, 99–108

Bostick, B.C., Fendorf, S., 2003. Arsenite sorption on troilite (FeS) and pyrite (FeS2). Geochimica et Cosmochimica Acta, 67, 909–921.

Boussafir, M., Lallier-Vergès, E., 1997. Accumulation of organic matter in the Kimmeridge Clay Formation (KCF); an update fossilisation model for marine petroleum source-rocks. Marine and Petroleum Geology, 14, 75-83.

Bout-Roumazeilles, V., Cortijo, E., Labeyrie, L., Debrabant, P., 1999. Clay mineral evidence of nepheloid layer contributions to the Heinrich layers in the northwest Atlantic. Palaeogeography, Palaeoclimatology, Palaeoecology 146, 211–228.

Boyer, C., Clark, B., Jochen, V., Lewis, R., Miller, C.K., 2011. Shale gas: a global resource. Oilfield Review 23, 28–39.

Breier, J.A., Toner, B.M., Fakra, S., Manganini, S.J., White, S.N., Thurnherr, A.M., German, C.R., 2012. Sulfur, sulfides, oxides, and organic matter aggregated in the deep-sea hydrothermal plumes 551 of 9° 50' N East Pacific Rise. Geochimica et Cosmochimica Acta, 88, 216- 236.

Brumsack, H.J., 2006. The trace metal content of recent organic carbon-rich sediments: implications for Cretaceous black shale formation. Palaeogeography Palaeoclimatology Palaeoecology 232, 344 –361.

Burchette, T.P., Wright, V.P., 1992. Carbonate ramp depositional systems. In B. W. Sellwood (Editor), Ramps and Reefs. Sedimentary Geology, 79, 3-57.

Carignan, J., Hild, P., Mevelle, G., Morel, J., Yeghicheyan, D., 2001. Routine analyses of trace element in geological samples using flow injection and low pressure on-line liquid chromatography coupled to ICP-MS: a study of geochemical reference materials BR, DR-N, UB-N, AN-G and GH. Geostandards Newsletter, Volume 25, pages 187–198.

Chaillou, G., Schäfer, J., Anschutz, P., Lavaux, G., Blanc, G., 2003. The behaviour of Arsenic in the muddy sediments of the Bay of Biscay (France). Geochimica et Cosmochimica Acta, 67, 2993-3003.

Chamley, H., 1989. Clay sedimentology. Springer-Verlag. Berlin Heidelberg, Germany, 623 pp.

Chappaz, A., Gobeil, C., Tessier, A., 2008. Geochemical and anthropogenic enrichments of Mo in sediments from perennially oxic and seasonally anoxic lakes in Eastern Canada. Geochim. Cosmochim. Acta 72, 170-184.

Couture, R-M., Gobeil, C, Tessier, A., 2010. Arsenic, iron and sulfur co-diagenesis of in lake sediments. Geochimica et Cosmochimica Acta, 74, 1238-1255.

Crusius, J., Calvert, S., Pedersen, T., Sage, D., 1996. Rhenium and molybdenum enrichments in sediments as indicators of oxic, suboxic, and sulfidic conditions of deposition. Earth and Planetary Science Letters 145, 65–78.

Cutter, G.A., Cutter, L.S., Featherstone, A.M., Lohrenz, S.E., 2001. Antimony and arsenic biogeochemistry in the western Atlantic Ocean. Deep-Sea Res. II, 48, 2895-2915.

Dale, A.W., Meyers, S.R., Aguilera, D.R., Arndt, S., Wallmann, K., 2012. Controls on organic carbon and molybdenum accumulation in Cretaceous marine sediments from the Cenomanian–Turonian interval including Oceanic Anoxic Event 2. Chemical Geology, 324–325, 28-45.

Deconinck, J.-F., 1993. Clay mineralogy of the Upper Tithonian-Berriasian deep-sea carbonates of the Vocontian Trough (SE France) : relationships with sequence stratigraphy. Bull. Centres Rech. Explor.-Prod. Elf-Aquitaine, 17, 1, p. 223-234.

Dellwig, O., Leipe, T., März, C., Glockzin, M., Pollehne, F., Schnetger, B., Yakushev, E.V., Böttcher, M.E., Brumsack, H.J., 2010. A new particulate Mn–Fe–P-shuttle at the redoxcline of anoxic basins. Geochimica et Cosmochimica Acta, 74, 7100-7115.

Digregorio, J.H., 1972. Neuquén. In: Leanza, A.F. (Ed.), Geología Regional Argentina. Academia Nacional de Ciencias, Córdoba, pp. 139–505.

Digregorio, J. H., Uliana, M. A., 1980. Cuenca Neuquina. In J. C. M.Turner (Ed.), Geología regional argentina (Vol. 2) (pp. 985 – 1032). Segundo Simposio de Geología Regional Argentina, Córdoba: Academia Nacional de Ciencias.

Durand, B., Monin, J.C., 1980. Elemental analysis of kerogens (C,H, O, N, S, Fe). In: Durand, B. (Ed.) Kerogen. pp. 113-142.

Embry, A.F., Johannessen, E.P., 1992. T–R, facies analysis and reservoir distribution in the uppermost Triassic- Lower Jurassic succession, western Sverdrup basin, Arctic Canada. In: Vorren, T.O., Bergsager, E., Dahl-Stamnes, O.A., Holter, E., Johansen, B., Lie, E., Lund, T.B. (Eds.), Arctic Geology and Petroleum Potential, vol. 2 (Special Publication). Norwegian Petroleum Society (NPF), pp. 121–146.

Espitalié, J., Deroo, G. Marquis, F., 1985. La pyrolyse Rock-Eval et ses applications ; première partie. Revue de l'Institut Français du Pétrole, 40, 563-579.

Franzese, J.R., Spalletti, L.A., 2001. Late Triassic - Early Jurassic continental extension in southwestern Gondwana: tectonic segmentation and pre break-up rifting. Journal of South American Earth Sciences 14:257-270.

Giusiano, A., Alonso, J., Chebli, G., Ibáñez, G., 2011. Gas no convencional en la cuencaNeuquina. El shale gas en la provincia del Neuquén. Informe de la Subsecretaría de Hidrocarburos, Energía y Minería, Gobierno de la Provincia del Neuquén, 54 pp.

Goldberg, T., Archer, C., Vance, D., Poulton, S.W.,2009. Mo isotope fractionation during adsorption to Fe (oxyhydr) oxides. Geochimca Cosmochimica Acta 73, 6502–6516.

Grabowski, J., Schnyder, J., Sobien, K., Koptíková, L., Krzeminski, L., Pszczó1kowski, A., Hejnar,J., Schnabl, P., 2013. Magnetic susceptibility and spectral gamma logs in the Tithonian-Berriasian pelagic carbonates in the Tatra Mts (Western Carpathians, Poland): Palaeoenvironmental changes at the Jurassic/Cretaceous boundary. Cretaceous Research, 43, p. 1-17.

Gradstein, F.M., Ogg, J. G., Schmitz. M.D., Ogg, G.M., 2012. The geologic time scale. Voluime 1. Elsevier Publications.

Groeber, P., 1946. Observaciones geológicas a lo largo del meridiano 70. Hoja Chos Malal. Revista de la Sociedad Geológica Argentina 1 (3), 177–208.

Groeber, P., 1953. Mesozoico. In: Geografía de la República Argentina, tomo 2: 1-541. Edited by the Sociedad Argentina de Estudios Geográficos (GAEA).

Gulisano, C.A., Gutiérrez Pleimling, A.R., Digregorio, R.E., 1984. Análisis estratigráfico del intervalo Tithoniano – Valanginiano (Formaciones Vaca Muerta, Quintuco y Mulichinco) en el suroeste de la provincia de Neuquén. 9º Congreso Geológico Argentino, Actas 1:221-235.

Helz, G.R., Bura-Nakić, E., Mikac, N., Ciglenečki, I., 2011. New model for molybdenum behavior in euxinic waters. Chemical Geology, 284, 323–332.

Howell, J.A., Schwarz, E., Spalletti, L.A., Veiga, G.D., 2005. The Neuquén Basin: an overview. In: Veiga, G.D., Spalletti, L.A., Howell, J., Schwarz, E. (Eds.): The Neuquén Basin: A Case Study in Sequence Stratigraphy and Basin Dynamics. Geological Society, Special Publications, 252, pp. 1-14.

Hu, Y., Feng, D., Peckmann, J., Roberts, H.H., Chen, D., 2014. New insights into cerium anomalies and mechanisms of trace metal enrichment in authigenic carbonate from hydrocarbon seeps. Chemical Geology, 381, 55–66.

Huerta-Diaz, M.A., Morse, J.W., 1992. Pyritization of trace metals in anoxic marine sediments. Geochimica et Cosmochimica Acta, 56, 2681–2702.

Jilbert, T., Slomp, C.P., 2013. Iron and manganese shuttles control the formation of authigenic phosphorus minerals in the euxinic basins of the Baltic Sea. Geochimica Cosmochimica Acta 107, 155-169

Kashiwabara, T., Takahashi, Y., Tanimizu, M., Usui, A., 2011. Molecular-scale mechanisms of distribution and isotopic fractionation of molybdenum between seawater and ferromanganese oxides. Geochimica Cosmochimica Acta 75, 5762-5784.

Kietzmann, D.A., Palma, R.M., Riccardi, A.C., Martín-Chivelet, J., López-Gómez, J., 2014. Sedimentology and sequence stratigraphy of a Tithonian–Valanginian carbonate ramp (Vaca Muerta Formation): A misunderstood exceptional source rock in the Southern Mendoza area of the Neuquén Basin, Argentina. Sedimentary Geology 302, 64–86.

Krim, N., 2015. Architecture stratigraphique, dynamique sédimentaire et distribution de la matière organique de la formation de la Vaca Muerta (Bassin de Neuquén, Argentine). Thèse de Doctorat. Université de Pau et des Pays de l'Adour.(France).

Krim, N., Bonnel, C, Tribovillard, N. Riboulleau, A., Imbert, P., Bout-Roumazeilles, V., Fasentieux, B., Hoareau, G., Aubourg, C., 2017. Paleoenvironmental evolution of the southern Neuquén Basin (Argentina) during Tithonian-Berriasian times (Vaca Muerta and Picún Leufú Formations): a multi-proxy approach. Bulletin de la Société Geologique de France, 188, 34.

Lafargue, E., Marquis, F., Pillot, D., 1998. Rock-Eval 6 applications in hydrocarbon exploration, production, and soil contamination studies. Revue de l'Institut Français du Pétrole, 53/4, 421– 437.

Leanza, H.A., 1980. The Lower and Middle Tithonian Ammonite fauna from Cerro Lotena, Province of Neuquén, Argentina. Zitteliana 5: 1-49. München.

Leanza, H.A., 1973. Estudio sobre los cambios faciales de los estratos limítrofes Jurasico-Cretácicos entre Loncopué y Picún Leufú, provincia del Neuquén, República Argentina. Revista de la Asociación Geológica Argentina 28, 97-132.

Leanza, H.A., Zeiss, A., 1990. Upper Jurassic lithostrtigraphic Limestone from Argentina (Neuquén Basin): Stratigraphy and Fossils. Facies, 22: 169-186.

Leanza, H.A., Zeiss, A., 1992. On the ammonite fauna of Lithostratigraphic Limestones from the Zapala region (Neuquen province, Argentina), with the description of a new genus. Zentralblat für Geologie und Paläontologie, 6: 1841-1850. Stuttgart.

Leanza, H.A., Marchese, H.G., Riggi, J.C., 1977. Estratigrafía del Grupo Mendoza con especial referencia a la Formación Vaca Muerta entre los paralelos 35º y 40º l.s. Cuenca Neuquina-Mendocina. Revista de la Asociación Geológica Argentina 32 (3): 190-208.

Leanza, H. A., Hugo, C. A., Repol, D., Salvarredy Aranguren, M., 2003. Miembro Huncal (Berriasiano inferior): un episodio turbidítico en la Formación Vaca Muerta, Cuenca Neuquina, Argentina. Revista de la Asociación Geológica Argentina. Volume 25, N° 2. Buenos Aires.

Legarreta, L., Gulisano, C., 1989. Análisis estratigráfico secuencial de la Cuenca Neuquina (Triásico superior-Terciario inferior). In: Chebli, G., Spalletti, L. A. (Eds.), Cuencas Sedimentarias Argentinas, Serie Correlación Geológica 6, S.M. de Tucumán, pp. 221-243.

Legarreta, L., Uliana, M.A., 1991. Jurassic-Cretaceous marine oscillations and geometry of backarc basin fill, Central argentine Andes. In: Macdonald, D. I. (Ed.), Sedimentation, Tectonics and Eustasy. Sea level Changes at Active Plate Margins. International Association of Sedimentologists Special Publication, Oxford 12, pp. 429-450.

Legarreta, L., Uliana, M.A., 1996a. La sucesión jurásica en el centrooeste de Argentina. Arreglo estratigráfico, secuencias y evolución paleogeográfica. Boletín de Informaciones Petroleras XII: 45, 66- 78.

Legarreta, L., Uliana, M.A., 1996b. The Jurassic succession in west-central Argentina: stratal patterns, sequences and palaeogeographic evolution. Palaeogeography, Palaeoclimatology, Palaeoecology 120:303-330.

Little, S.H., Vance, D., Lyons, T.W., McManus, J., 2015. Controls on trace metal authigenic enrichment in reducing sediments: insights from modern oxygen-deficient settings. American Journal of Science, 315, 77–119.

Macdonald, D., Gómez Pérez, I., Franzese, J., Spalletti, L., Lawver, L., Gahagan, L., Dalziel, I., Thomas, C., Trewin, N., Hole, M., Paton, D., 2003. Mesozoic break-up of SW Gondwana: implications for regional hydrocarbon potential of the southern South Atlantic. Marine and Petroleum Geology 20:287-308.

Manceda, R., Figueroa, D., 1995. Inversion of the Mesozoic Neuquén Rift in the Malargüe Fold and Thrust Belt, Mendoza, Argentina. In: Tankard, A.J., Suárez Soruco, R., Welsink, H.J. (Eds.) Petroleum Basins of South America, American Association of Petroleum Geologist Memoir 62, pp. 369-382.

Marchese, H.G., 1971. Litoestratigrafía y variaciones faciales de las sedimentitas mesozoicas de la Cuenca Neuquina, Prov. de Neuquén, Rep. Argentina. Asociación Geológica Argentina Revue V. 26, pp. 343-410.

Martin, P., van der Loeff, M.R., Cassar, N., Vandromme, P., d'Ovidio, F., Stemmann, L., Rengarajan, R., Soares, M., González, H.E., Ebersbach, F., Lampitt, R.S., Sanders, R., Barnett, B.A., Smetacek, V., Naqvi, S.W.A., 2013. Iron fertilization enhanced net community production but not downward particle flux during the Southern Ocean iron fertilization experiment LOHAFEX. Glob. Biogeochem. Cycles 27, 871-881. http://dx.doi.org/10.1002/gbc.20077.

Massaferro, J.L., Zeller, M., Giunta, D.L., Sagasti, G., Eberli, G.P., 2014. Evolución del sistema mixto tithoniano-valanginiano (Formaciones Vaca Muerta, Quintuco y equivalentes) a partir de estudios de afloramientos y subsuelo, centro- sur de la Cuenca Neuquina. IX Congreso de Exploración y Desarrollo de Hidrocarburos.

McLennan, S.M., 2001. Relationships between the Trace Element Composition of Sedimentary Rocks and Upper Continental Crust. Geochemistry, Geophysics, Geosystems, 2.

Minami, H., Kato, Y., 1997. Remobilization of arsenic in sub-oxic sediments from seafloor of the continental margin. J. Ocenaogr., 53, 553–562.

Mitchum, R.M., Uliana, M.A., 1985. Seismic stratigraphy of carbonate depositional sequences. Upper Jurassic/Lower Cretaceous. Neuquén Basin, Argentina. In: Berg, B.R., Woolverton, D.G. (Eds.), Seismic Stratigraphy, II. An Integrated Approach to Hydrocarbon Analysis. American Association of Petroleum Geologists, Memoir 39, 255-274.

Mosquera, A., Ramos, V.A., 2006. Intraplate deformation in the Neuquén Embayment. In: Kay, S.M., Ramos, V.A. (Eds.), Evolution of an Andean margin: a tectonic and magmatic view from the Andes to the Neuquén Basin (35°–39° lat): Geological Society of America Special Paper 407, pp. 97–124.

Naipauer, M., García Morabito, E, Marques, J.C., Tunik, M., Rojas Vera, E.A., Vujovich, G.I., Pimentel, M.P., Ramos, V.A., 2012. Intraplate Late Jurassic deformation and exhumation in western central Argentina: Constraints from surface data and U–Pb detrital zircon ages. Tectonophysics 524–525, 59–75.

Nesbitt, H.W., 2003. Petrogegenesis of siliciclastic sediments and sedimentary rocks. In Lentz, D.R. ed., Geochemistry of Sediments and Sedimentary Rocks: Evolutionary Considerations to Mineral Deposit-Forming Environments. Geol. Assoc. Canada GeoText4, 39-51.

Neumann, T., Scholz, F., Kramar, U., Ostermaier, M., Rausch, N., Berner, Z., 2013. Arsenic in framboidal pyrite from recent sediments of a shallow water lagoon of the Baltic Sea. Sedimentology, doi: 10.1111/sed.12031.

O'Day, P., 2006. Chemistry and mineralogy of arsenic. Elements, 2, 77-83.

Owens, J.D., Lyons, T.W., Li, X., Macleod, K.G., Gordon, G., Kuypers, M.M.M., Anbar, A., Kuhnt, W., Severmann, S., 2012. Iron isotope and trace metal records of iron cycling in the proto-North Atlantic during the Cenomanian-Turonian oceanic anoxic event (OAE-2). Paleoceanography 27, PA3223. http://dx.doi.org/10.1029/2012PA002328.

Pángaro, F., Veiga, R., Vergani, G., 2002. Evolución tecto-sedimentaria del área de Cerro Bandera, Cuenca Neuquina, Argentina. 5º Congreso Argentino de Exploración de Hidrocarburos, Mar del Plata, Abstracts on CD.

Parent, H., Garrido, A., Scweigert, G., Sherzinger, A., 2013. The Tithonian stratigraphy and ammonite fauna of the transect Portada Covunco-Cerrito Caracoles (Neuquén Basin, Argentina). N. Jb. Geol. Paläont. Abh. 269/1 (2013), 1–50 Article. Schweizerbart'sche Verlagsbuchhandlung, Stuttgart.

Passey, Q.R., Bohacs, K.M., Esch, W.L.,. Klimentidis, R.E.., Sinha,S., 2010, From oil-prone source rock to gas-producing shale reservoir – geologic and petrophysical characterization of unconventional shale-gas reservoirs: SPE 131350, 29 p.

Petsch, S.T., Berner, R.A., Eglinton, T.I., 2000. A field study of the chemical weathering of ancient sedimentary organic matter. Organic Geochemistry, 31, 475-487.

Quattrocchio, M., Sarjeant, W.A.S., 1992. Dinoflagellate cysts and acritarchs from the Middle and Upper Jurassic of the Neuquén Basin, Argentina. Revista Española de Micropaleontología. 24. 67-118.

Ramos, V. A., 1999b. Evolución tectónica de la Argentina. In: Caminos, R. (Ed.) Geología Argentina Servicio Geológico Minero Argentino, Buenos Aires, Anales 29, pp. 715-784.

Ruffell, A.H., Price, G.D., Mutterlose, J., Kessels, K., Baraboshkin, E., Gröcke, D.R., 2002. Palaeoclimate indicators (clay minerals, calcareous nannofossils, stable isotopes) compared from two successions in the late Jurassic of the Volga basin (SE Russia). Geological Journal, 37, p. 17-33.

Schnyder, J., Ruffell, A., Deconinck, J.-F., Baudin, F., 2006. Conjunctive use of spectral gamma-ray logs and clay mineralogy in defining late Jurassic-early Cretaceous palaeoclimate change (Dorset, U.K.). Palaeogeography, Palaeoclimatology, Palaeoecology, 229, p. 303-320.

Scholz, F., Hensen, C., Noffke, A., Rohde A., Liebetrau, V., Wallmann, K., 2011. Early diagenesis of redox-sensitive trace metals in the Peru upwelling area – response to ENSO-related oxygen fluctuations in the water column. Geochimica Cosmochimica Acta, 75, 7257-7276.

Scholz, F., McManus, J., Sommer, S., 2013. The manganese and iron shuttle in a modern euxinic basin and implications for molybdenum cycling at euxinic ocean margins. Chemical Geology, 335, 56-68.

Scott, C., Lyons, T.W., 2012. Contrasting molybdenum cycling and isotopic properties in euxinic versus non-euxinic sediments and sedimentary: refining the paleoproxies. Chemical Geology, 324-325, 19-27.

Spalletti, L.A., Colombo Piñol, F., 2005. From alluvial fan to playa: an Upper Jurassic ephemeral fluvial system, Neuquén Basin, Argentina. Gondwana Research 8 (3), 363–383.

Spalletti, L.A., Veiga, G.A., 2007. Variability of continental depositional systems during lowstand sedimentation: an example from the Kimmeridgian of the Neuquén Basin, Argentina. Latin American Journal of Sedimentology and Basin Analysis | vol. 14 (2), 85-104.

Spalletti, L.A., J. Franzese, S.D. Matheos, Schwarz, E., 2000. Sequence stratigraphy in tidally-dominated carbonate-siliciclastic ramp, the Tithonian of the southern Neuquén Basin, Argentina. Journal of the Geological Society 157:433-446.

Sullivan, K.A., Aller, R.C., 1996. Diagenetic cycling of arsenic in Amazon shelf sediments. Geochim. Cosmochim. Acta, 60, 1465–1477.

Taylor, S.R., McLennan, S.M., 1985. The continental crust: its composition and evolution. Blackwell Scientific Publication, Carlton, 312 p.

Tissot, B.P., Welte, D.H., 1978. Petroleum Formation and Occurrence. Springer-Verlag, Berlin, 522p.

Tribovillard, N., Ramdani, A., Trentesaux, A., 2005. Controls on organic accumulation in Late Jurassic shales of Northwestern europe as inferred from trace-metal geochemistry. In Harris, N. (ed.) The Deposition of Organic-Carbon-Rich Sediments: Models, Mechanisms, and Consequences. SEPM Spec. Public., 82, ISBN 1-56576-110-3, 145-164.

Tribovillard, N., Algeo, T., Lyons, T.W., Riboulleau, A., 2006. Trace metals as paleoredox and paleoproductivity proxies: an update. Chemical Geology, 232, 12–32.

Tribovillard, N., Algeo, T.J., Baudin, F., Riboulleau, A., 2012. Analysis of marine environmental conditions based on molybdenum–uranium covariation—Applications to Mesozoic paleoceanography. Chemical Geology 324-325, pp 46–58.

Tribovillard, N., Armynot du Châtelet, E., Gay, A., Barbecot, F., Sansjofre, P., Potdevin, J.-L., 2013. Geochemistry of cold seepage-impacted sediments: Per-ascensum or per-descensum trace metal enrichment? Chemical Geology, 340, 1-12.

Tribovillard, N., Hatem, E., Averbuch, O., Barbecot, F., Bout-Roumazeilles, V., Trentesaux, A., 2015. Iron availability as a dominant control on the primary composition and diagenetic overprint of organic-matter-rich rocks. Chemical Geology, 401, 67-82.

Tyson, R.V., 2005. The "productivity versus preservation" controversy; cause, flaws, and resolution. In: Harris, N.B. (Ed.), Deposition of Organic-carbon-rich Sediments: Models, Mechanisms, and Consequences. Society for Sedimentary Geology (SEPMSSG) Special Publication 82, pp. 17–33.

Tyson, R.V., 1995. Sedimentary organic matter. Chapman & Hall, London,616p.

Van der Weijden, C.H., 2002. Pitfalls of normalization of marine geochemical data using a common divisor. Mar. Geol. 184, 167–187.

Vaughan, D.J., 2006. Arsenic. Elements, 2, 71-75.

Vergani, G., Tankard, A.J., Belotti, H.J., Welsink, H. J., 1995, Tectonic evolution and paleogeography of the Neuquen Basin, Argentina, In A.J. Tankard, R. Suarez, S., and H. J. Welsink. Petroleum basins of South America: AAPG Memoir 62, 383-402.

Veiga, R., Verzi, H., Maretto, H., 2001. Modelado bidimensional en el ámbito central de la cuenca Neuquina (Argentina). Boletín de Informaciones Petroleras XVIII, 67:50-63.

Walker, R.G., Plint, A.G., 1992. Wave- and storm-dominated shallow marine systems. In: Walker, R.G., James, N.P. (Eds.), Facies Models: Response to Sea Level Change, pp. 219–238.

Weaver, C., 1931. Paleontology of the Jurassic and Cretaceous of west central Argentina. University of Washington, Seattle, Memoir 1, 469 pp.

Yrigoyen, M.R., 1991. Hydrocarbon resources from Argentina. World Petroleum Congress, Buenos Aires. Petrotecnia, 13, Special issue, 38-54.

Zavala, C., Maretto, H., Di Meglio, M., 2005. Hierarchy of bounding surfaces in Aeolian sandstones of the Tordillo Formation (Jurassic). Neuquén Basin, Argentina. Geologica Acta 3, 133–145.

Tables :

Table 1: Average clay mineral composition showing the main differences between the Picún Leufú and Covunco areas.

Mean ± standard deviation	% Chlorite	% Illite	% IS14C-14S	% IS10-14S	% Smectite	% Kaolinite
Section 1	2 ±3	11 ±7	-	3 ±5	76 ±17	8 ±6
Section 2	2 ±3	5 ±4	-	3 ±4	83 ±13	7 ±6
Section 3	2 ±6	6 ±4	-	2 ±8	74 ±22	16 ±21
Section 4	2 ±2	7 ±6	-	4 ±4	78 ±13	10 ±6
Section 5	1 ±1	7 ±4	0±1	3 ±3	83 ±9	5 ±6
COVUNCO	6 ±10	21 ±16	-	8 ±9	56 ±32	8 ±12

Figure captions:

Figure 1: A. Location map of the Neuquén Basin. B. Isopach map showing the main depocentres during the Kimmeridgian times, and location of the main structures (Huincul Arch, Chihuidos High) (After Vergani et al., 1995, Spalletti and Colombo Pinol, 2005, Spalletti and Veiga, 2007). C. Zoom of Picún Leufú and Covunco sections

Figure 2: Tectonostratigraphic chart of the southern Neuquén Basin and adjacent sectors showing main unconformities and timing of deformation (Naipauer et al. 2012).

Figure 3: Chronostratigraphic chart of the Tithonian – Early Valanginian in the southern and central Neuquén Basin (Modified after Spalletti, 2000). Huncal Member from Leanza et al., 2003. Time scale of Gradstein et al., 2012.

Figure 4: Lithological log and location of the samples of the studied outcrops in the Picún Leufú Anticline and Covunco area. a. Age (from Leanza 1980; Leanza and Zeiss, 1990; Leanza and Zeiss 1992. Parent et al., 2013). b. Name of formations. c. Depositionnal environnements (Krim, 2015 ; Krim et al., 2017). d. Sequence stratigraphy (Krim, 2015 ; Krim et al., 2017). Log sections of Picún Leufú area, mineralogical and geochemical data of section #3 are also taken from Krim et al. (2017). Red points indicate sample location.

Figure 5: Clay mineral distribution in the study area. Sections 1 to section 5 correspond to the Picún Leufú area. % C: % Chlorite, % I: % Illite, % IS14-14S: % Illite-Smectite mixed layer, % S: % Smectite, % K: % Kaolinite. a. Age (from Leanza; 1980; Leanza and Zeiss, 1990; Leanza and Zeiss 1992. Parent et al., 2013). b. Name of formations. c. Depositionnal environnements (Krim, 2015 ; Krim et al., 2017). d. Sequence stratigraphy (Krim, 2015 ; Krim et al., 2017). Log sections of Picún Leufú area, mineralogical and geochemical data of section #3 are also taken from Krim et al. (2017). Red points indicate sample location.

Figure 6: Average clay distribution of each sampled log section in the Picún Leufú and Covunco areas.

Figure 7: Ternary diagrams illustrating clay mineral distribution for the studied sections.

Figure 8: Chemical Index Alteration (CIA) distribution (%) and chlorite-kaolinite ratio in the Picún Leufú and Covunco areas. Notice the reverse scale of the two proxies.

Figure 9. U–EF vs. Mo–EF crossplot of the study interval in Picún Leufú and Covunco area. The general patterns of U–EF vs. Mo–EF covariation in modern marine environments is

illustrated above (Algeo and Tribovillard, 2009): The grey field represents the “unrestricted marine”, characteristic of the eastern tropical Pacific, whereas the yellow field represents the “particulate shuttle” trend, characteristic of depositional systems such as the Cariaco Basin in which intense redox cycling of metal especially Mn− oxyhydroxides occurs within the water column.

Figure 10: Total organic carbon (TOC, blue) and Hydrogen Index (HI, red) values in the Picún Leufú and Covunco areas. Lithological logs as in Figure 4. a. Age (from Leanza; 1980; Leanza and Zeiss, 1990; Leanza and Zeiss 1992. Parent et al., 2013). b. Name of formations. c. Depositionnal environnements (Krim, 2015 ; Krim et al., 2017). d. Sequence stratigraphy (Krim, 2015 ; Krim et al., 2017).

Figure 11: A. Plot of Hydrogen Index (HI) versus Oxygen Index (OI) showing Kerogen Type of the study interval in Picún Leufú and Covunco areas. B. Plot of Hydrogen Index (HI) versus pyrolysis Tmax showing Kerogen Type and thermal maturity stages of the study interval, in Picún Leufú and Covunco areas.

Figure 12: A. Plot of Hydrogen Index (HI) versus total organic carbon (TOC) for the different sections of Picún Leufú and Covunco areas. B. Plot of Tmax versus Oxygen Index (OI) comparing Covunco area and Picún Leufú area.

Figure 13: Total organic carbon contents vs. Mo concentrations ([TOC] vs. [Mo]) diagrams drawn for each section. The solid lines represent four present-day basins characterized by some restriction of the water mass circulation. The restriction severity increases from the Saanich Inlet to the Black Sea. See explanations in Algeo and Lyons (2006) and Algeo et al. (2007).The four settings used as reference (Saanich Inlet, Cariaco Basin, Framvaren Fjord and Black Sea) are characterized by increasing water mass restriction due to hydrological conditions. This restriction limits the dissolved Mo resupply from open sea, which may lead to its exhaustion in case of massive transfer from the water column down to the sediment.

Figure 14: Lithology, sequence stratigraphy and Rock-Eval parameters distribution (vertical TOC, Hydrogen Index (HI), Oxygen Index (OI)) in section 5 showing the location of the richest TOC intervals. a. Age (from Leanza; 1980. Parent et al., 2013). b. Name of formations. c. Depositional environnements (Krim, 2015 ; Krim et al., 2017). d. Sequence

stratigraphy (Krim, 2015 ; Krim et al., 2017). e. Detailed sequence stratigraphy (Krim et al., 2017).

Figure 1

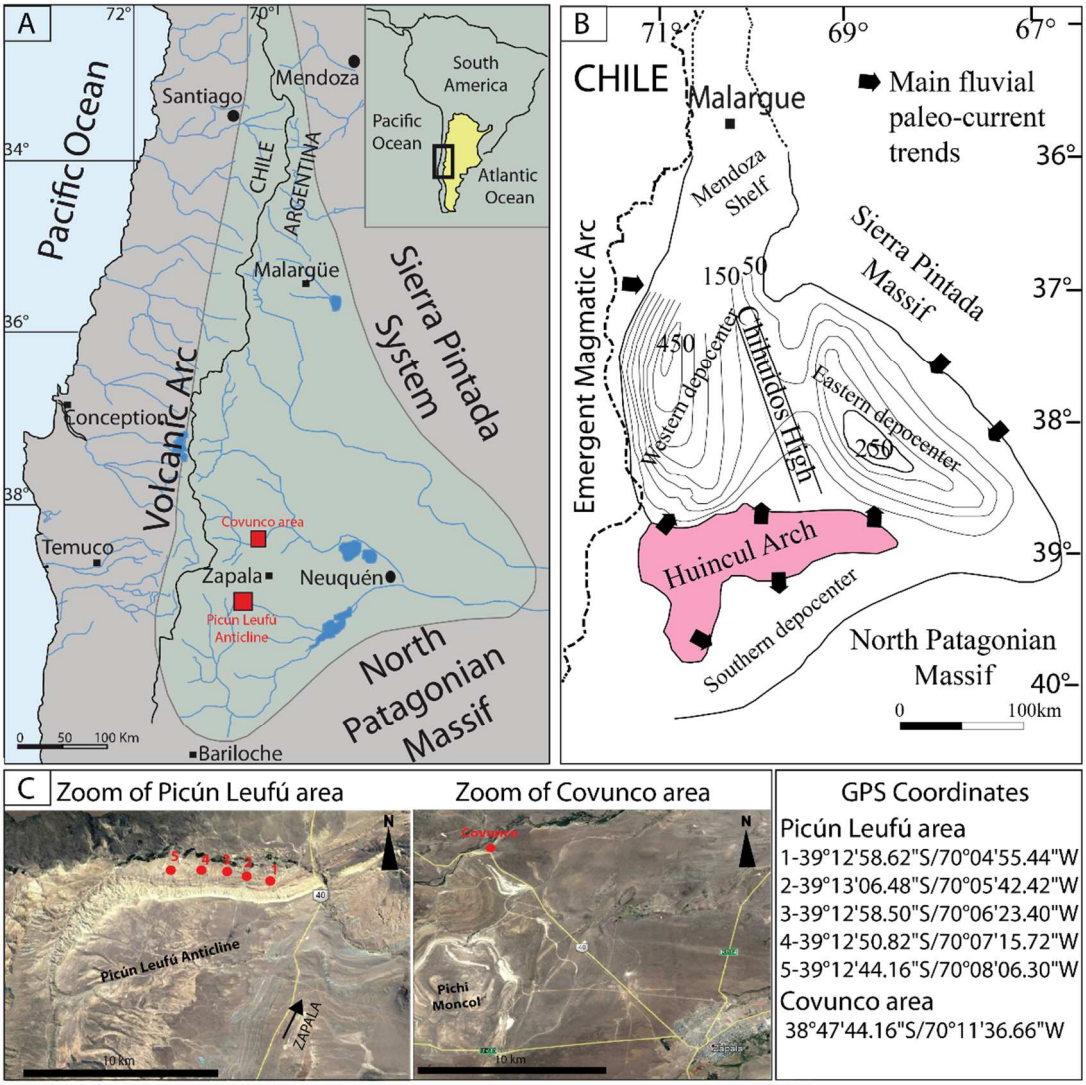
A
72°
70°
34°
36°
38°
Pacific Ocean
Santiago
Mendoza
CHILE
ARGENTINA
Malargüe
Sierra Pintada System
Volcanic Arc
Concepción
Temuco
Covunco area
Zapala
Neuquén
Picún Leufú Anticline
North Patagonian Massif
Bariloche
0 50 100 Km
South America
Pacific Ocean
Atlantic Ocean
B
71°
69°
67°
CHILE
Malargue
Main fluvial paleo-current trends
36°
Mendoza Shelf
Sierra Pintada Massif
37°
150
50
450
Western depocenter
Chihuidos High
Eastern depocenter
250
Emergent Magmatic Arc
38°
Huincul Arch
39°
Southern depocenter
North Patagonian Massif
40°
0 100km
C
Zoom of Picún Leufú area
Zoom of Covunco area
N
Picún Leufú Anticline
ZAPALA
10 km
Covunco
Pichi Moncol'
GPS Coordinates
Picún Leufú area
1-39°12'58.62"S/70°04'55.44"W
2-39°13'06.48"S/70°05'42.42"W
3-39°12'58.50"S/70°06'23.40"W
4-39°12'50.82"S/70°07'15.72"W
5-39°12'44.16"S/70°08'06.30"W
Covunco area
38°47'44.16"S/70°11'36.66"W

Figure 2

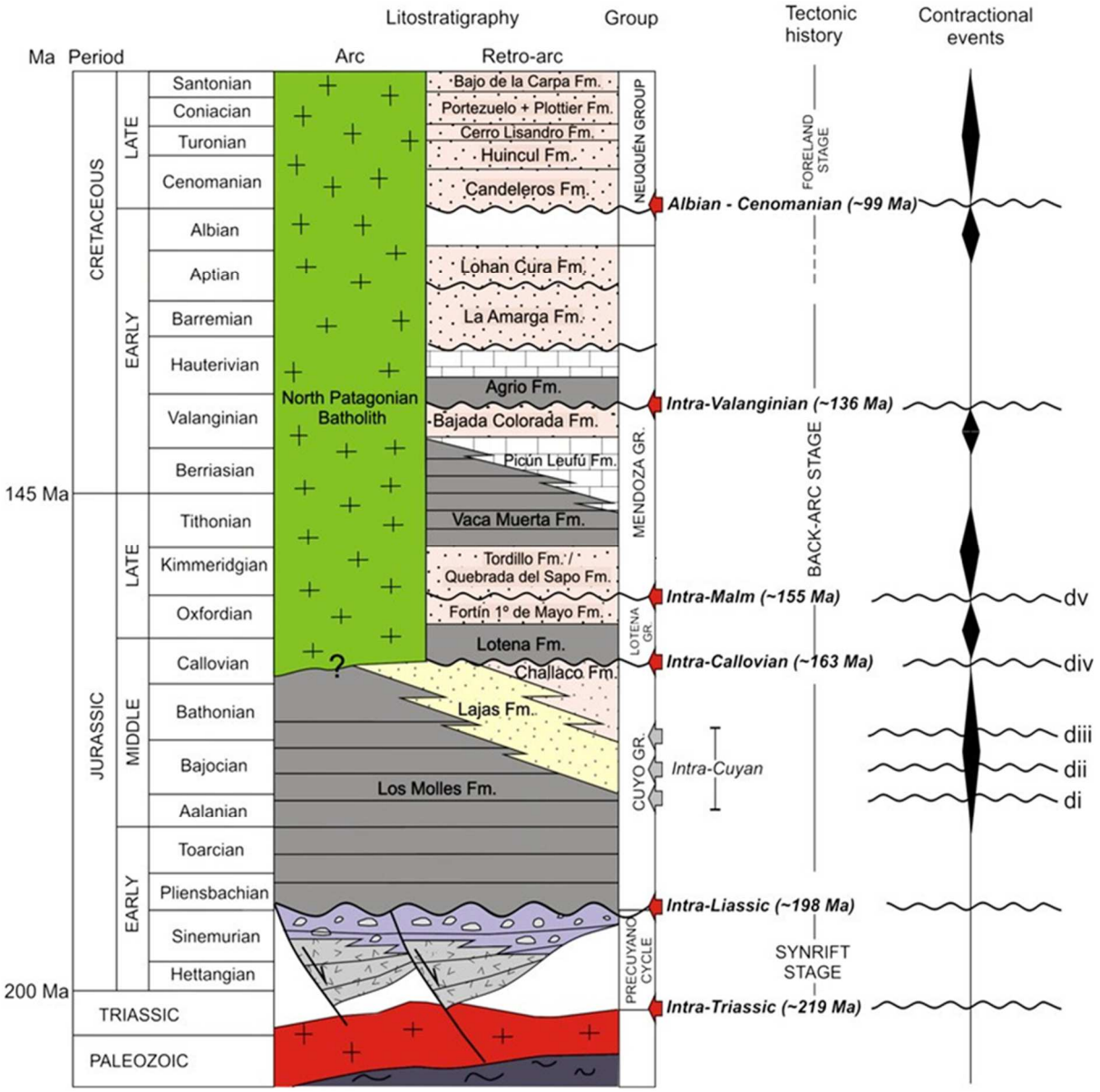
Litostratigraphy
Group
Tectonic history
Contractional events
Ma
Period
Arc
Retro-arc
CRETACEOUS
JURASSIC
TRIASSIC
PALEOZOIC
LATE
EARLY
MIDDLE
Santonian
Coniacian
Turonian
Cenomanian
Albian
Aptian
Barremian
Hauterivian
Valanginian
Berriasian
Tithonian
Kimmeridgian
Oxfordian
Callovian
Bathonian
Bajocian
Aalanian
Toarcian
Pliensbachian
Sinemurian
Hettangian
145 Ma
200 Ma
North Patagonian Batholith
Bajo de la Carpa Fm.
Portezuelo + Plottier Fm.
Cerro Lisandro Fm.
Huincul Fm.
Candeleros Fm.
Lohan Cura Fm.
La Amarga Fm.
Agrio Fm.
Bajada Colorada Fm.
Picún Leufú Fm.
Vaca Muerta Fm.
Tordillo Fm. / Quebrada del Sapo Fm.
Fortín 1° de Mayo Fm.
Lotena Fm.
Challaco Fm.
Lajas Fm.
Los Molles Fm.
NEUQUÉN GROUP
MENDOZA GR.
LOTENA GR.
CUYO GR.
PRECUYANO CYCLE
Intra-Cuyan
FORELAND STAGE
BACK-ARC STAGE
SYNRIFT STAGE
Albian - Cenomanian (~99 Ma)
Intra-Valanginian (~136 Ma)
Intra-Malm (~155 Ma)
Intra-Callovian (~163 Ma)
Intra-Liassic (~198 Ma)
Intra-Triassic (~219 Ma)
dv
div
diii
dii
di

Figure 3

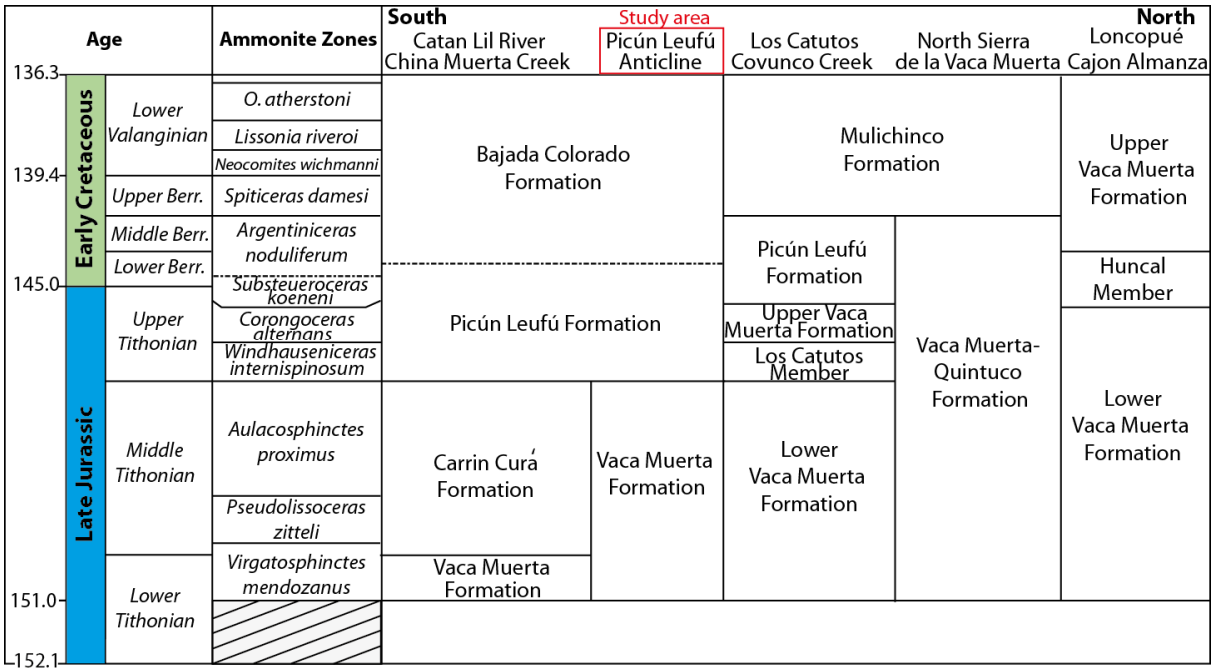
Age
Ammonite Zones
South
Catan Lil River
China Muerta Creek
Study area
Picún Leufú
Anticline
Los Catutos
Covunco Creek
North Sierra
de la Vaca Muerta
North
Loncopué
Cajon Almanza
136.3
139.4
145.0
151.0
152.1
Early Cretaceous
Late Jurassic
Lower Valanginian
Upper Berr.
Middle Berr.
Lower Berr.
Upper Tithonian
Middle Tithonian
Lower Tithonian
O. atherstoni
Lissonia riveroi
Neocomites wichmanni
Spiticeras damesi
Argentiniceras noduliferum
Substeueroceras koeneni
Corongoceras alternans
Windhauseniceras internispinosum
Aulacosphinctes proximus
Pseudolissoceras zitteli
Virgatosphinctes mendozanus
Bajada Colorado Formation
Picún Leufú Formation
Carrin Curá Formation
Vaca Muerta Formation
Vaca Muerta Formation
Mulichinco Formation
Picún Leufú Formation
Upper Vaca Muerta Formation
Los Catutos Member
Lower Vaca Muerta Formation
Vaca Muerta-Quintuco Formation
Upper Vaca Muerta Formation
Huncal Member
Lower Vaca Muerta Formation

Figure 4

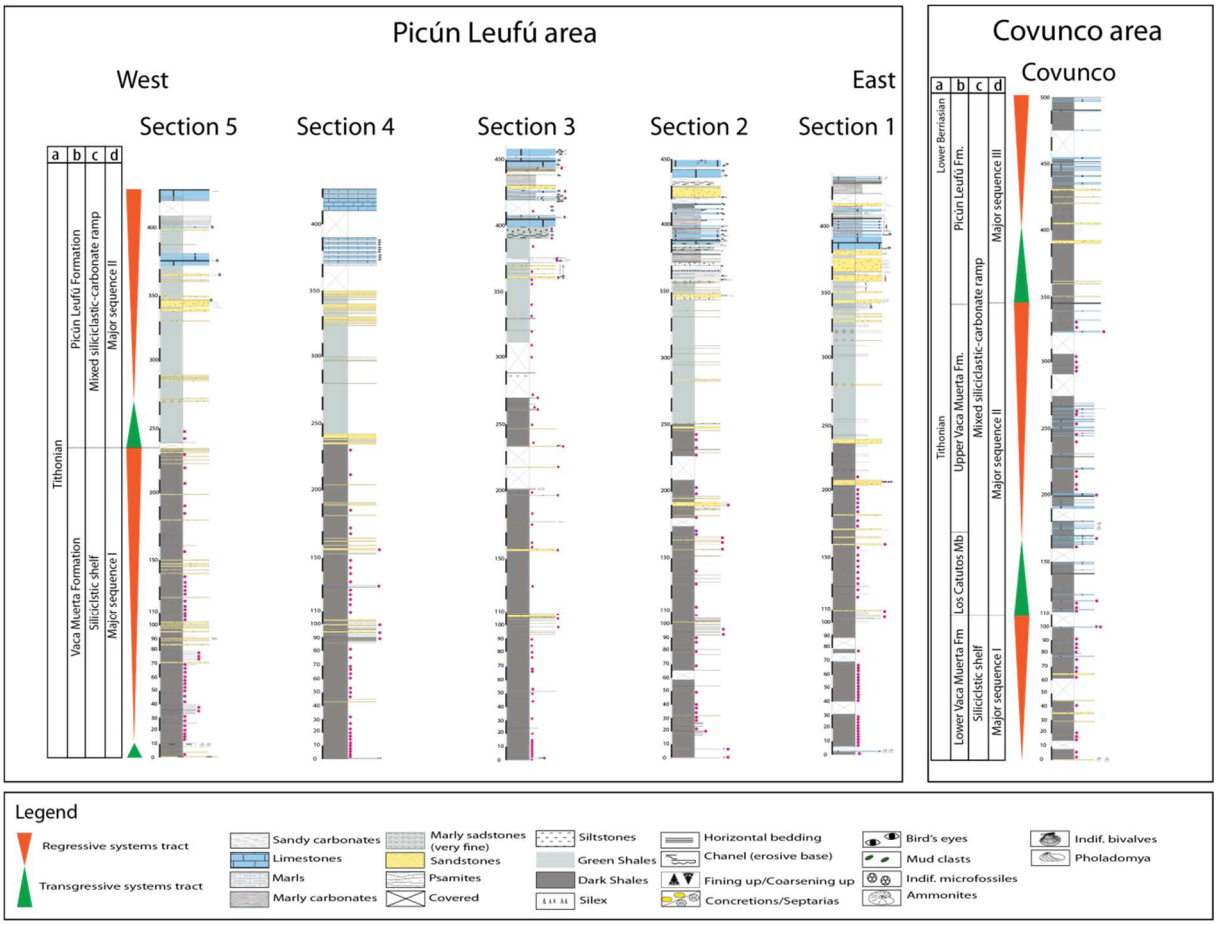
Picún Leufú area
West
East
Section 5
Section 4
Section 3
Section 2
Section 1
a
b
c
d
Tithonian
Vaca Muerta Formation
Picún Leufú Formation
Siliciclstic shelf
Mixed siliciclastic-carbonate ramp
Major sequence I
Major sequence II
Covunco area
Covunco
Lower Berriasian
Tithonian
Lower Vaca Muerta Fm
Los Catutos Mb
Upper Vaca Muerta Fm.
Picún Leufú Fm.
Siliciclstic shelf
Mixed siliciclastic-carbonate ramp
Major sequence I
Major sequence II
Major sequence III
Legend
Regressive systems tract
Transgressive systems tract
Sandy carbonates
Limestones
Marls
Marly carbonates
Marly sadstones (very fine)
Sandstones
Psamites
Covered
Siltstones
Green Shales
Dark Shales
Silex
Horizontal bedding
Chanel (erosive base)
Fining up/Coarsening up
Concretions/Septarias
Bird's eyes
Mud clasts
Indif. microfossiles
Ammonites
Indif. bivalves
Pholadomya

Figure 5

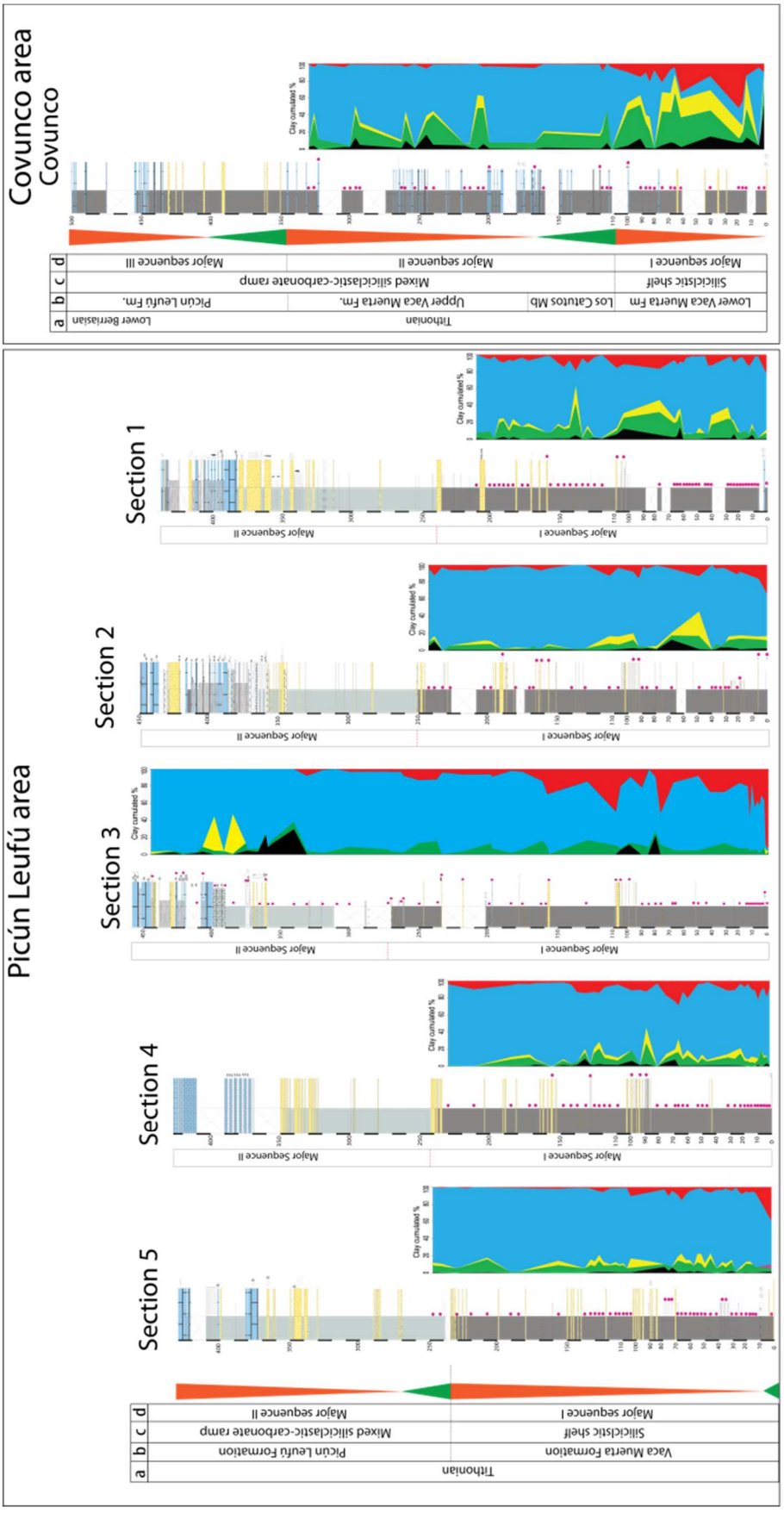
Covunco area
Covunco
Clay cumulated %
Major sequence I
Major sequence II
Major sequence III
Tithonian
Lower Berriasian
Lower Vaca Muerta Fm
Los Catutos Mb
Upper Vaca Muerta Fm.
Picún Leufú Fm.
Siliciclastic shelf
Mixed siliciclastic-carbonate ramp
Picún Leufú area
Section 1
Section 2
Section 3
Section 4
Section 5
Vaca Muerta Formation
Picún Leufú Formation
%C
%I
%IS14-14S
%IS10C-14S
%S
%K

Figure 6

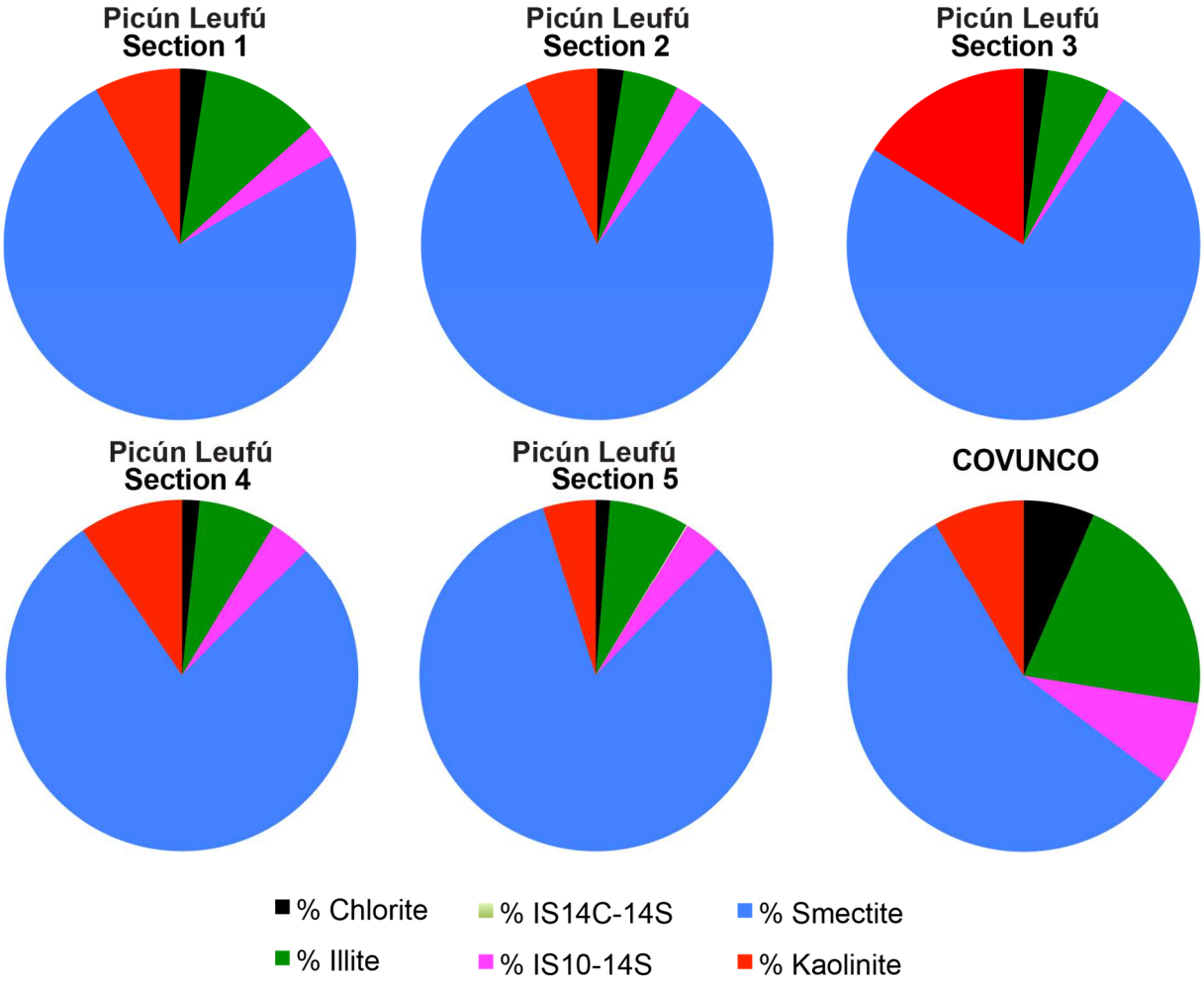
Picún Leufú
Section 1
Picún Leufú
Section 2
Picún Leufú
Section 3
Picún Leufú
Section 4
Picún Leufú
Section 5
COVUNCO
% Chlorite
% IS14C-14S
% Smectite
% Illite
% IS10-14S
% Kaolinite

Figure 7

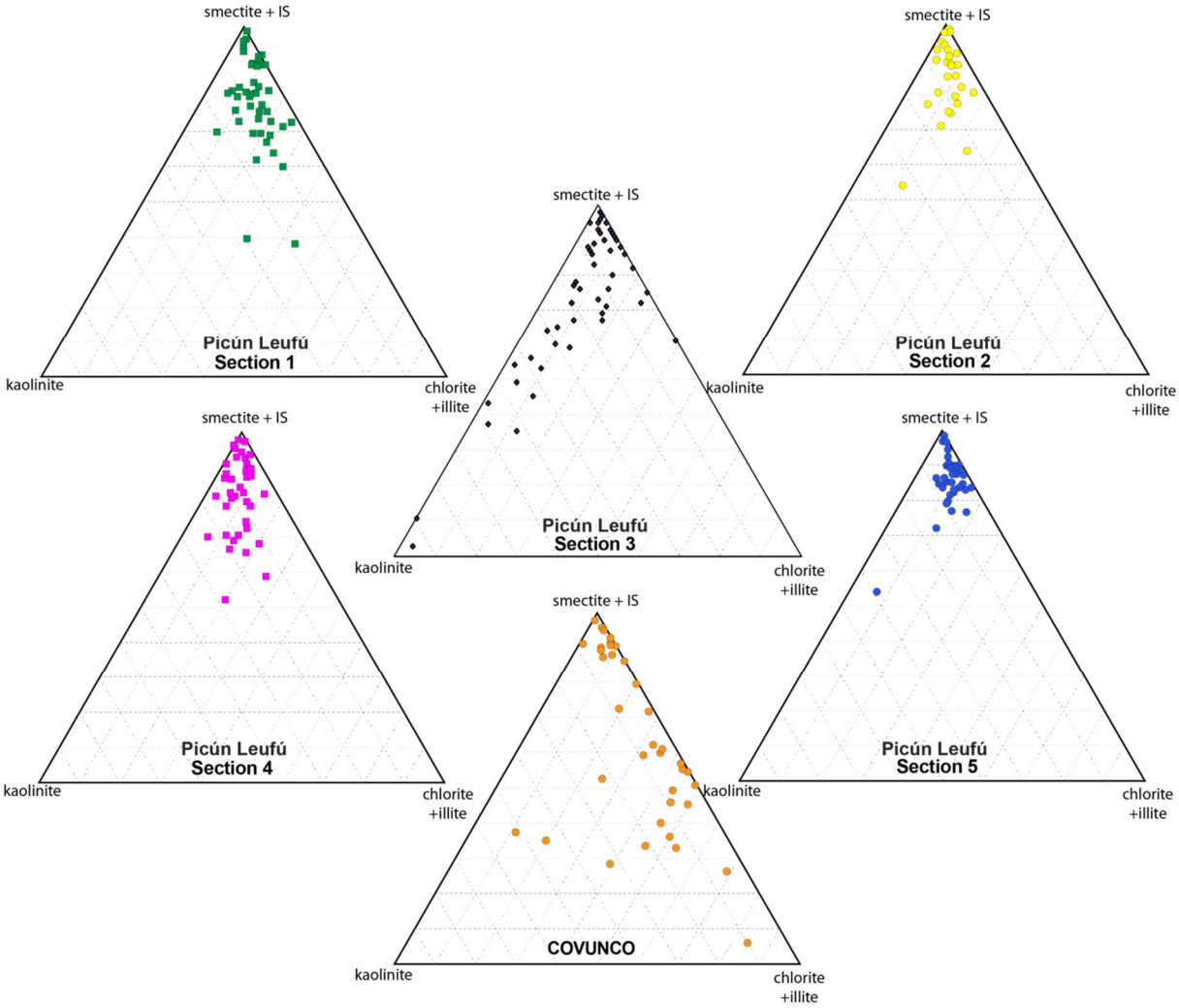
smectite + IS
kaolinite
chlorite +illite
Picún Leufú Section 1
Picún Leufú Section 2
Picún Leufú Section 3
Picún Leufú Section 4
Picún Leufú Section 5
COVUNCO

Figure 8

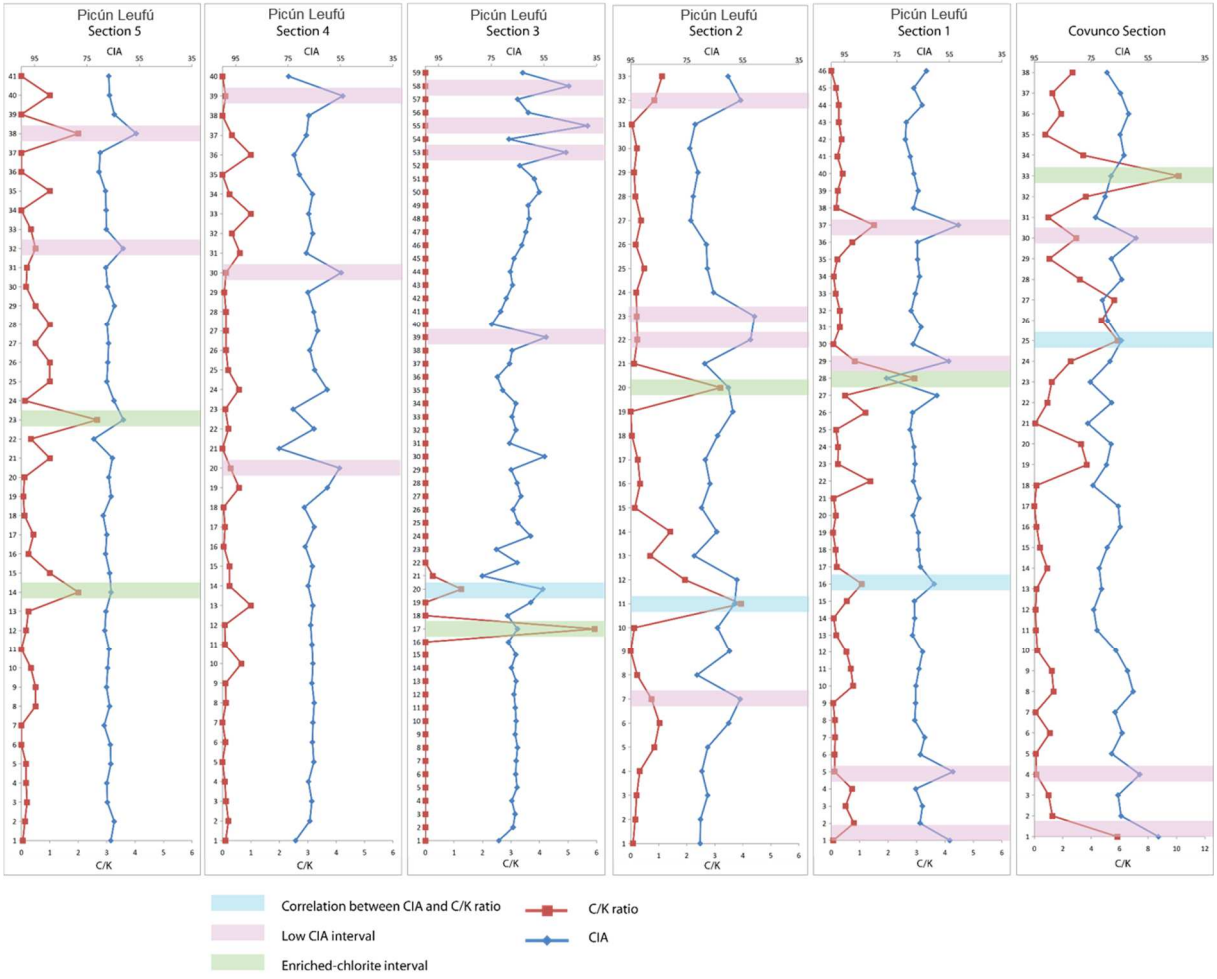
Picún Leufú Section 5
Picún Leufú Section 4
Picún Leufú Section 3
Picún Leufú Section 2
Picún Leufú Section 1
Covunco Section
CIA
C/K
Correlation between CIA and C/K ratio
Low CIA interval
Enriched-chlorite interval
C/K ratio
CIA

Figure 9

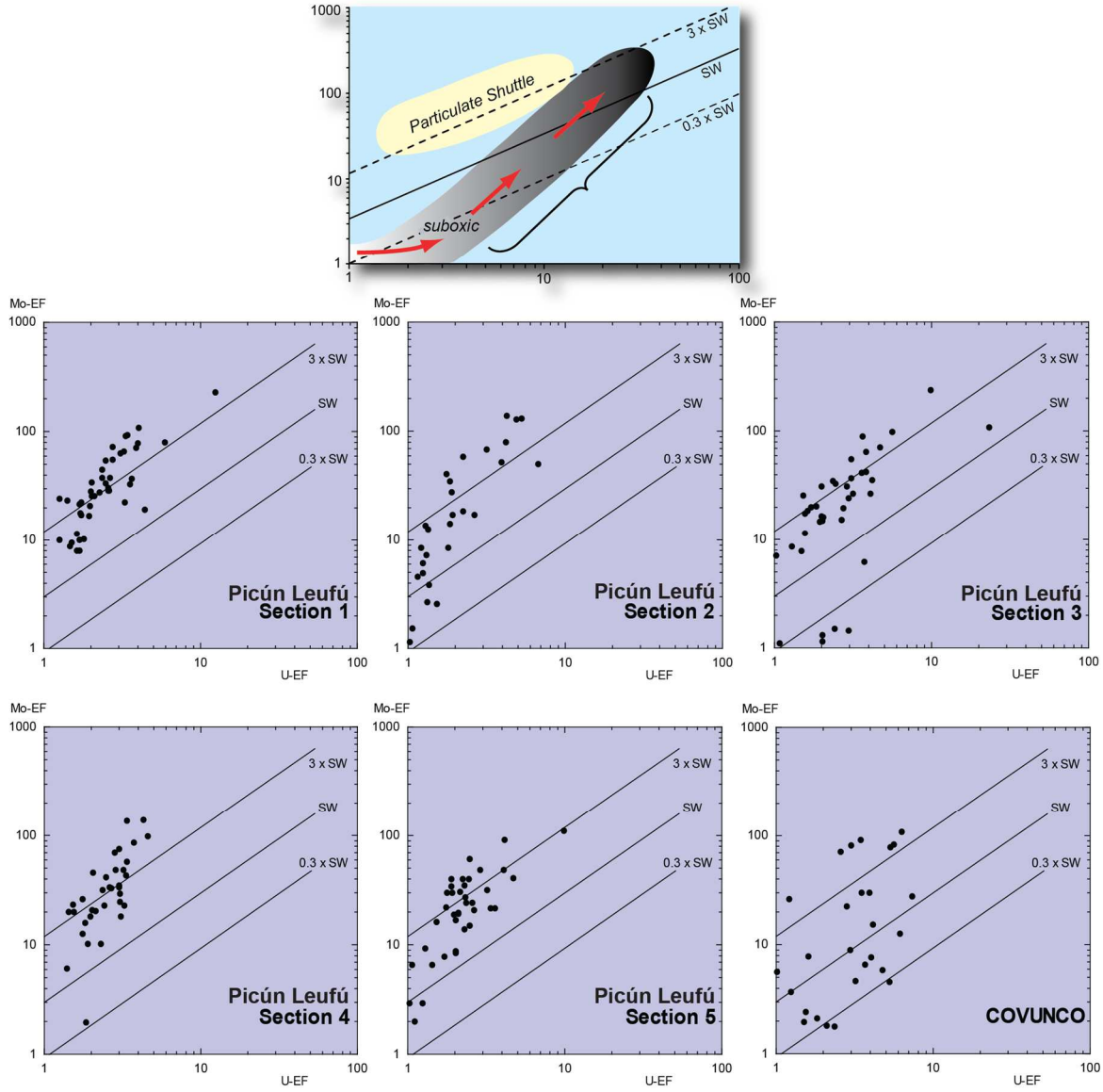
Particulate Shuttle
suboxic
3 x SW
SW
0.3 x SW
Mo-EF
U-EF
Picún Leufú
Section 1
Picún Leufú
Section 2
Picún Leufú
Section 3
Picún Leufú
Section 4
Picún Leufú
Section 5
COVUNCO

Figure 10

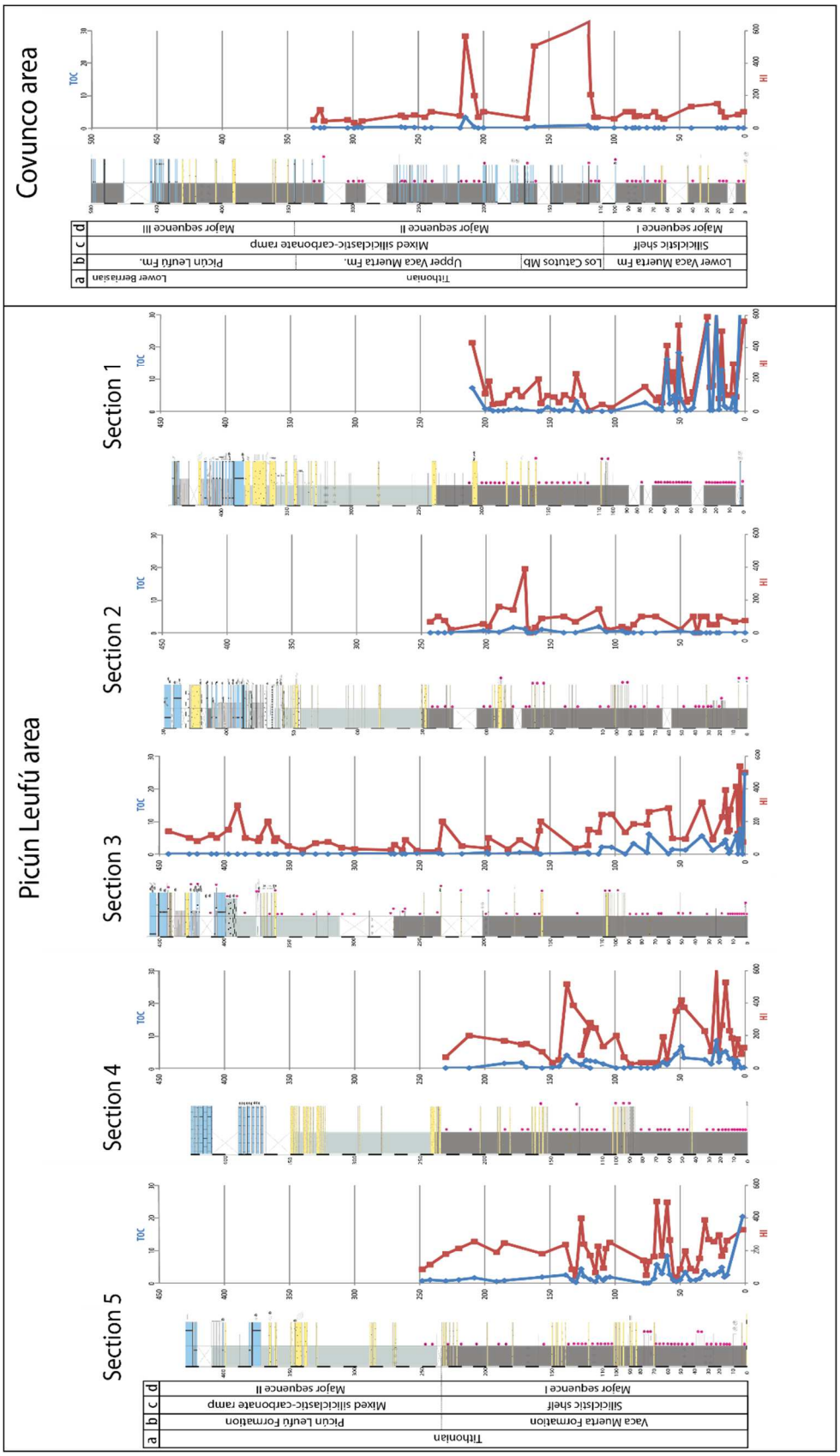
Covunco area
Picún Leufú area
Section 1
Section 2
Section 3
Section 4
Section 5
TOC
HI
Tithonian
Lower Berriasian
Los Catutos Mb
Upper Vaca Muerta Fm.
Picún Leufú Fm.
Lower Vaca Muerta Fm
Silicic/Istic shelf
Mixed silicic/clastic-carbonate ramp
Major sequence I
Major sequence II
Major sequence III
Vaca Muerta Formation
Picún Leufú Formation
a
b
c
d

Figure 11

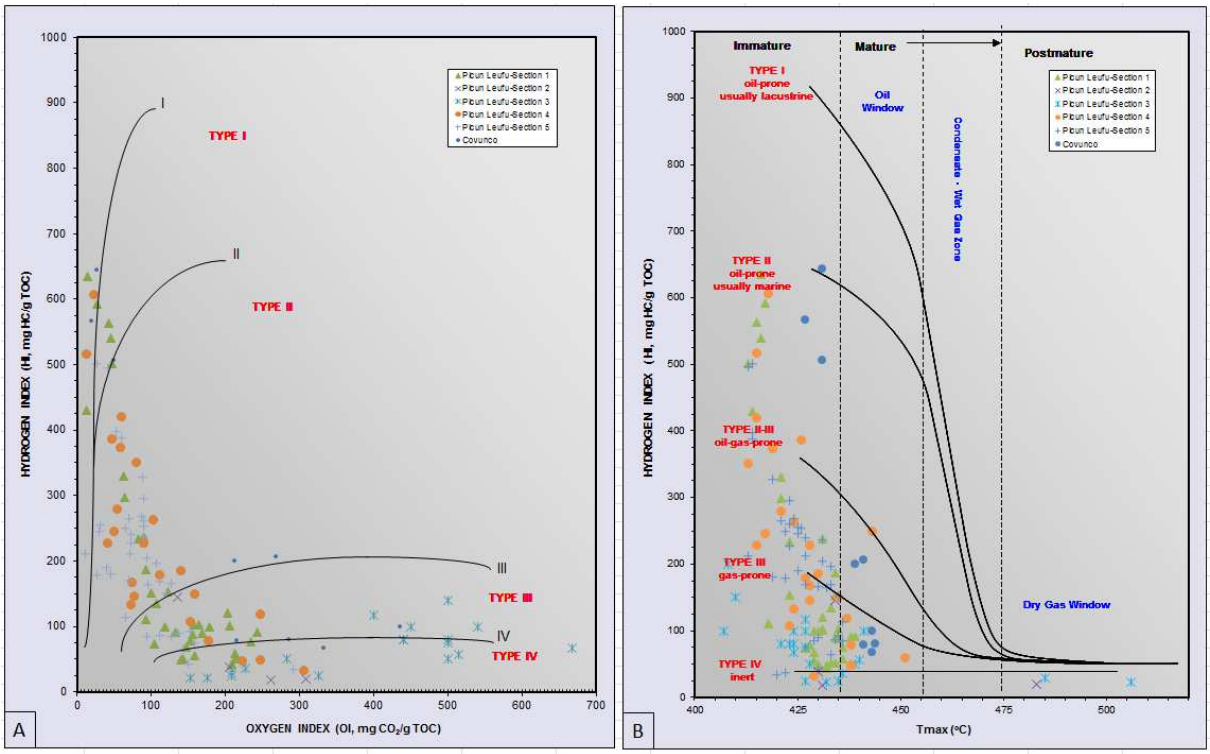
A
HYDROGEN INDEX (HI, mg HC/g TOC)
OXYGEN INDEX (OI, mg CO2/g TOC)
TYPE I
TYPE II
TYPE III
TYPE IV
Pbun Leufu-Section 1
Pbun Leufu-Section 2
Pbun Leufu-Section 3
Pbun Leufu-Section 4
Pbun Leufu-Section 5
Covunco
B
Immature
Mature
Postmature
TYPE I
oil-prone
usually lacustrine
Oil
Window
Condensate - Wet Gas Zone
TYPE II
oil-prone
usually marine
TYPE II-III
oil-gas-prone
TYPE III
gas-prone
TYPE IV
inert
Dry Gas Window
Tmax (°C)

Figure 12

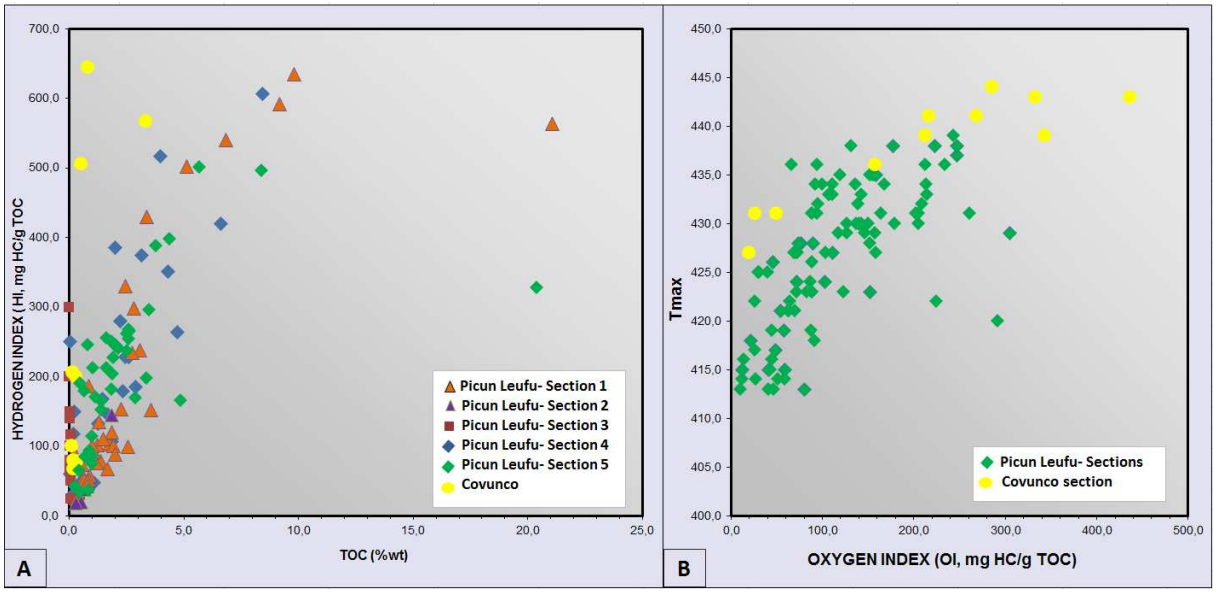
HYDROGEN INDEX (HI, mg HC/g TOC
TOC (%wt)
Picun Leufu- Section 1
Picun Leufu- Section 2
Picun Leufu- Section 3
Picun Leufu- Section 4
Picun Leufu- Section 5
Covunco
A
Tmax
OXYGEN INDEX (OI, mg HC/g TOC)
Picun Leufu- Sections
Covunco section
B

Figure 13

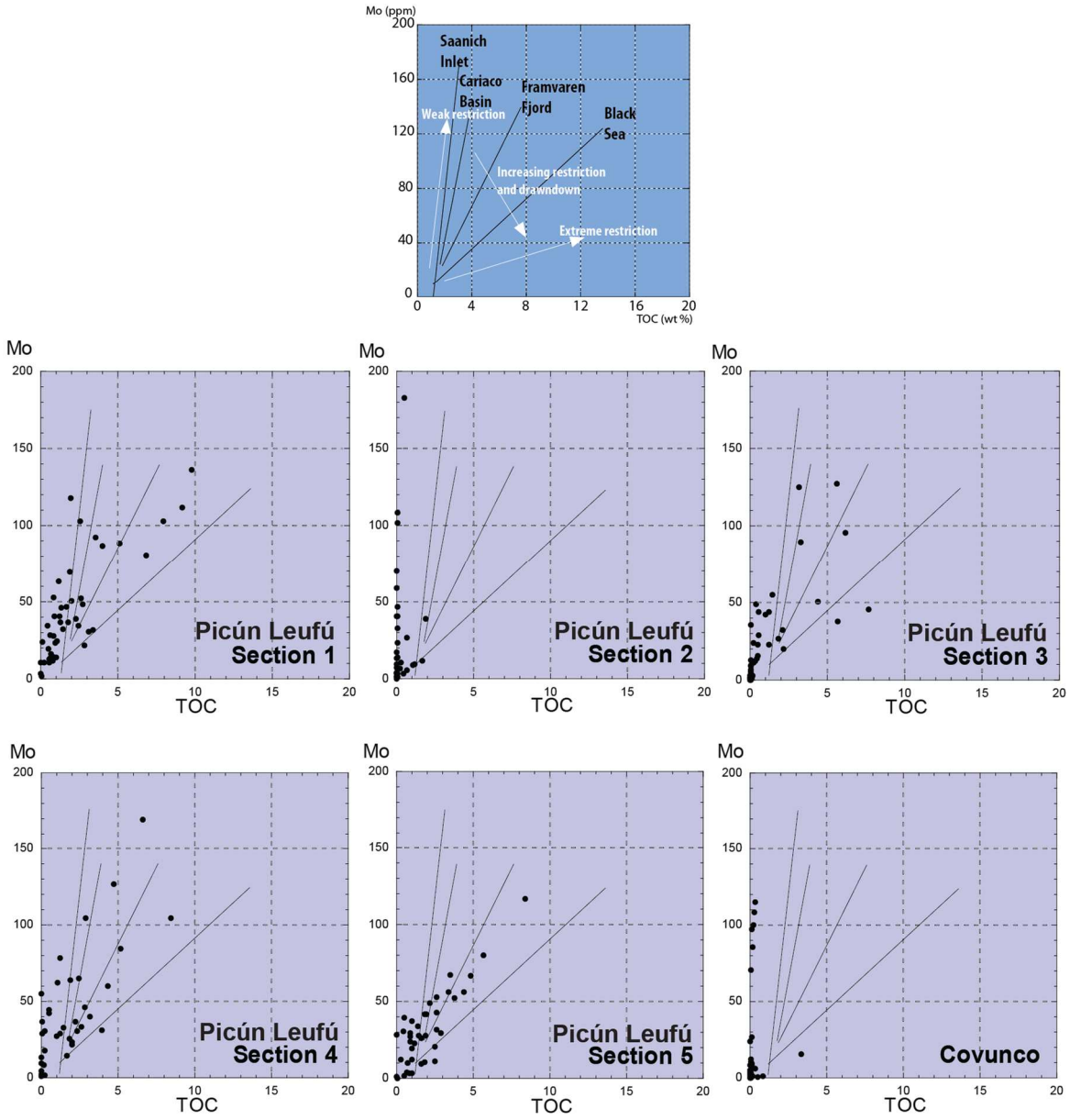
Mo (ppm)
Saanich Inlet
Cariaco Basin
Framvaren Fjord
Black Sea
Weak restriction
Increasing restriction and drawndown
Extreme restriction
TOC (wt %)
Mo
TOC
Picún Leufú Section 1
Picún Leufú Section 2
Picún Leufú Section 3
Picún Leufú Section 4
Picún Leufú Section 5
Covunco

Figure 14

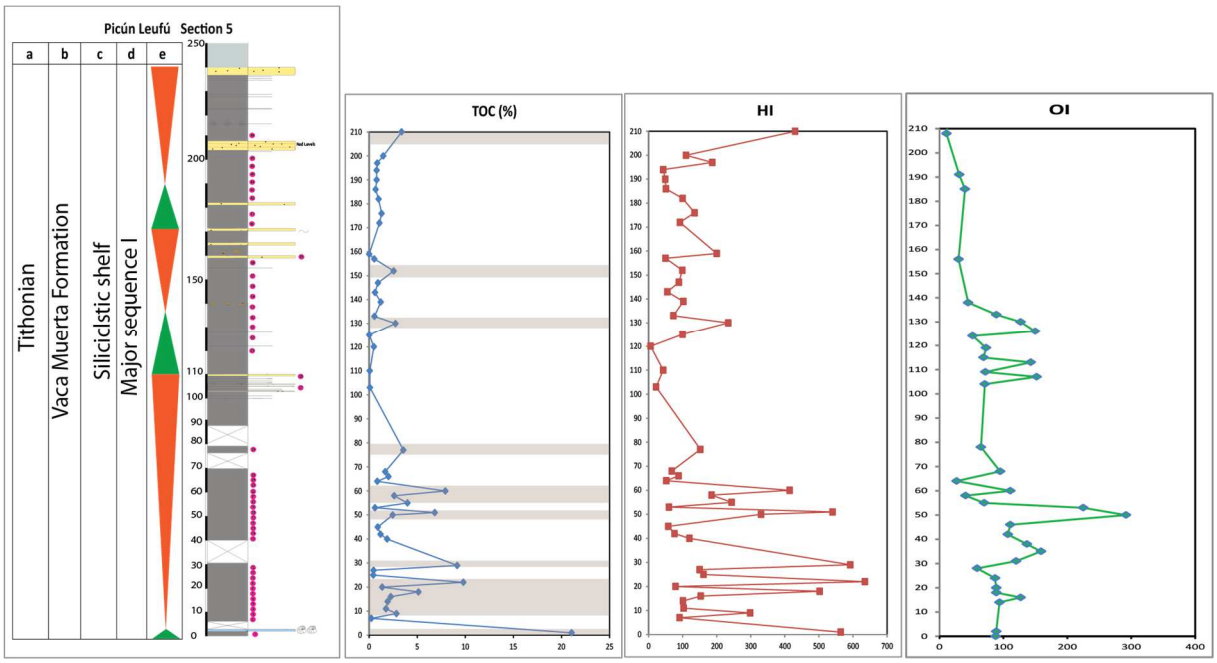
Picún Leufú Section 5
a
b
c
d
e
Tithonian
Vaca Muerta Formation
Siliciclstic shelf
Major sequence I
TOC (%)
HI
OI

Appendix 1. Paleo-productivity and Paleoredox proxies

Section1

Sample Name	Thickness (m)	Ba (ppm)	Cu (ppm)	Ni (ppm)	V EF	Zn EF	Mo EF	U EF	As EF	Sb EF	Pb EF
48	**210**	253,8	31,7	45,9	1	9,4	24,2	1,3	9,2	4,2	1,2
47	**200**	266,4	20	30,4	1	4,8	22,4	1,7	7,5	3,7	1,1
46	**197**	189,2	11,1	11,3	0,7	2,6	21,4	1,7	4,7	3,7	0,7
45	**194**	260,6	16,9	21,9	1	1,3	9,4	1,5	7,1	2,3	0,8
44	**190**	248,2	22,2	27	1,2	0,6	8	1,6	5,3	3	1,1
43	**186**	268,7	17,3	12,3	1,1	0,5	11,4	1,6	6,8	3	1,9
42	**182**	251	22,7	28	2	2,4	10	1,7	6,6	2,5	1
41	**176**	279,8	19,2	23,6	1,5	2,9	25,6	2	8,6	5,3	1,4
40	**172**	278,4	25,7	31,4	1,4	2,4	17,8	1,7	8,7	4,5	1,1
39	**159**	304,1	8,8	55,8	0,3	0,3	10,1	1,3	11,7	5,4	1,6
38	**157**	253,2	17,9	22,8	1,1	0,4	8	1,7	3,7	3,2	1,1
37	**152**	329,1	23,7	20,7	2,5	4,6	78,7	4	7,9	7,2	1,4
36	**147**	367,5	25,6	26,4	2	1,4	16,8	1,9	10,1	7,1	1,2
34	**143**	323,9	21,4	26,2	1,7	0,5	20,8	2	7,8	5,6	1,2
33	**139**	326,5	25,3	24	2	2,1	27,7	2,3	8,4	5,6	0,8
32	**133**	282,2	16,4	26,4	0,9	0,4	8,8	1,5	5,4	3,4	0,8
31	**130**	333,4	25,3	35,6	1,9	7,6	34,4	2	9,8	5,8	1,5
30	**125**	413,4	12,8	129,3	0,3	0,4	2,7	0,9	6,5	3,1	1
29	**120**	209,6	10,7	40,1	1,9	0,8	28,6	2,6	13,9	6	2
28	**110**	385,9	10,8	8,7	0,5	0,4	1,3	0,8	3,8	1,7	0,6
27	**103**	251,3	18,6	30,4	1,2	1,4	23,3	1,4	13,6	5,1	1,9
26	**77**	313,6	28	31,9	2,8	6,7	62,6	3,1	12,6	6,9	1,9
25	**68**	305,5	28,1	46,4	2,9	5,7	32,7	3,5	8,1	6,3	1,3
24	**66**	320,8	22,8	37,9	2,2	0,5	36,7	3,6	9,8	5,5	1,2
23	**64**	331,5	15,8	50,5	1,6	0,4	37,6	2,4	11	8,5	1
22	**60**	332,8	24,1	36,1	3,2	3,5	79	6	13,4	7,3	1,1
21	**58**	288,4	21	35,9	1,5	0,4	37,7	2,6	6,2	4	1
20	**55**	309,2	23,7	46,5	1,9	0,8	65,1	3,3	9,2	3,7	1,5
19	**53**	276,2	17,8	28,5	1,1	0,3	10,2	1,8	4,6	3,4	1,4
18	**51**	258,1	18	47,5	1,5	0,4	22,4	3,3	3,1	4,6	0,8

17	**50**	252,1	22,4	39,2	3,6	4,7	71,4	3,9	6,7	10,4	1,3
15	**45**	247,6	23,6	21,8	1,9	0,7	30,6	2,6	8,4	9,2	1,7
14	**42**	328,6	30,3	34,8	1,7	0,4	28,4	2	8,5	3,5	1,7
13	**40**	325,6	30,8	51,7	1,8	0,4	44,8	2,4	11,5	5,1	1,4
12	**29**	296,8	29,2	58,9	2,5	1,5	54,7	2,5	13	8,8	1,3
11	**27**	298,3	37,3	109,5	4,8	3,8	93,6	3,4	12,6	16	1,5
10	**25**	185,4	13,2	72,9	2,4	0,5	54,9	2,8	10,9	5,2	1,2
9	**22**	397,5	35,8	127,3	3,4	0,7	108,3	4	10,7	9	1,3
8	**20**	284,8	31,6	21,1	1,3	0,3	33,3	2,5	5	3,3	1
7	**18**	256,8	42,4	44,9	2,8	0,8	72,7	2,7	6,8	7	0,9
6	**16**	354,1	28,8	53,2	2	0,3	28,5	2,6	8,6	5,4	1,4
5	**14**	566,8	41,3	32,6	2,3	1,1	91	3,3	18	12,2	2,1
4	**11**	314,4	30,1	55,4	1,8	0,4	25,7	2,1	11,4	8,1	2,2
3	**9**	286,3	28,6	27,6	2,2	0,3	17,1	1,7	8,6	7,2	2
2	**7**	100,8	16,4	39,6	2,3	0,7	19,3	4,4	15,3	6,9	3,9
1	**1**	225,8	41	43,2	5,9	36,2	228,1	12,4	109,5	14,1	14,8

Section 2

Sample Name	Thickness (m)	Ba (ppm)	Cu (ppm)	Ni (ppm)	V EF	Zn EF	Mo EF	U EF	As EF	Sb EF	Pb EF
32	**243**	299,1	12,7	11,4	0,6	0,5	0,8	0,7	2,9	2	1
31	**237**	756	11,1	16,8	0,4	0,5	2,7	1,3	6,5	2,7	1,3
30	**232**	127	< L.D.	10,6	0,6	1,3	2,4	0,9	5	1	0,9
29	**227**	102,1	8,9	9,9	0,9	1,5	8,5	1,2	5,3	1	1,1
28	**202**	240,2	18,2	14,3	0,8	0,5	3,9	1,4	2,3	1,9	0,9
27	**198**	236,8	18,6	16,3	0,7	0,6	2,3	1	4,1	1,9	1,1
26	**190**	217,1	8,3	19,9	1,1	1,8	17,2	1,9	6,5	1	1,2
25	**179**	259,9	25,1	12,1	1	0,7	8,4	1,8	5,9	2,4	0,9
24	**170**	119,3	8	29,8	1,2	1	14,1	1,8	8,5	2,9	1,1
23	**168**	133,2	10,9	104,4	1	2	41	1,8	9,3	3,1	1
22bis	**166**	392,6	6,2	7,2	0,3	0,3	1,5	1,1	2,1	1,3	0,8
22	**162**	411,1	6,8	14,2	0,2	0,3	6,3	0,9	4,8	1,8	1

21	**157**	263,4	22,9	12,8	0,6	0,4	6	1,2	5,5	2,1	1,3
20	**140**	149,4	< L.D.	13	0,4	0,5	5	1,2	5	2,3	0,9
19	**131**	211,5	11,5	30,5	0,6	0,4	12,6	1,3	16,2	6	1,4
18	**113**	343,9	23,2	24,7	2,4	0,6	27,7	1,9	9	7,3	0,9
17	**107**	296,9	30,5	29,7	1,2	0,7	7,3	1,3	7,2	3,6	1
16	**95**	331,1	24,7	19,8	1,7	1,5	18,5	2,2	6,4	4,7	1,3
15	**92**	142,3	12,2	43,1	1,5	3,3	35	1,8	32,1	4,5	2
14	**90**	269,9	20,4	9,6	0,4	0,3	4,5	1,1	5,5	3,3	1,1
13	**86**	146,9	13,1	58,3	1,8	9,1	58,8	2,3	12,8	5,6	1,9
12	**80**	347,9	11,1	18,2	0,4	0,8	6,9	1	4,9	2	1,7
11	**69**	372,8	12,3	8	0,5	0,3	1,1	1	3,1	1,4	0,6
10	**50**	343,6	26,9	75,6	2,4	1,1	130,2	5,3	10,5	4,7	1
9	**40**	442,7	8	21,6	1,1	0,7	17	2,6	12,7	4,1	1
8	**37**	351,7	21,7	81,6	2,3	2,7	79,5	4,2	21,7	6,5	1,6
7	**34**	315,4	13,9	23,3	0,5	0,3	13,6	1,3	7,7	3,2	0,9
6	**30**	321,5	5,7	11,8	0,9	0,3	2,6	1,5	1	1,6	0,7
5	**27**	449,8	21,3	128,1	2,2	0,9	138,6	4,3	15,9	6,5	1,2
4	**22**	619,7	26,3	156,8	2,5	0,8	127,5	4,9	16,7	6,7	1,3
3	**20**	220,4	21,1	104,8	2	1,7	50,2	6,7	16,1	7,6	1,2
2	**8**	182,5	28,1	40,9	2,2	0,9	68,6	3,2	13,1	7,2	2,5
1	**0**	212,3	373,8	63,1	1,8	9,5	51,8	3,9	19,2	7,9	5,3

Section 3

Sample Name	Thickness (m)	Ba (ppm)	Cu (ppm)	Ni (ppm)	V EF	Zn EF	Mo EF	U EF	As EF	Sb EF	Pb EF
59	**443**	393,7	15,81	1	0,6	0	0,6	0,9	6,4	1,5	0,8
58	**427**	1014	1	1	0,3	0,5	0,1	0,9	0,9	0,7	0,4
57	**421**	287,6	5,926	9,151	0,5	0,4	0,7	2,2	4,5	0,7	0,8
56	**410**	292	1	8,1	0,5	0,3	1,2	2	4,1	2	1,1
55	**406**	575,1	5,722	6,654	0,5	0,4	1,4	3	6,1	1,9	1,2
54	**397**	418,8	22,71	8,201	0,9	0,9	0,1	0,9	0,7	4,3	0,4
53	**390**	575,5	1	1	0,3	0	0,1	0,5	1,5	0,6	0,6
52	**384**	433	5,907	1	0,4	0,5	0,5	1	2,2	1,2	0,7

51	**374**	97,73	1	6,953	0,6	48	1,5	2,4	11,1	2	1,4
50	**373**	314,3	1	5,345	0,4	0	0,9	0,7	4,7	1	1,6
49	**366,7**	372,3	9,234	7,021	0,4	0,3	0,9	0,8	2,1	1,4	1
48	**361,5**	218,2	1	9,685	0,4	3,8	1,3	2	9,6	2,9	1,4
47	**360**	252,5	7,569	8,871	0,4	0,4	1,4	0,9	4,7	1,9	1,2
46	**351**	296	11,22	7,872	0,5	0,4	0,6	0,8	3,1	1,7	1,1
45	**340**	693,1	18,65	20,69	0,5	0,5	1,5	0,8	6,5	2,8	2
44	**330**	852,5	9,88	8,724	0,4	0,4	1,3	0,9	4,2	2,2	1,5
43	**320,5**	394	10,25	20,75	0,5	0,4	1	0,9	3,2	1,7	1,1
42	**310**	384,4	10,33	6,994	0,5	0,3	1,6	0,9	2,9	1,9	1,1
41	**300**	264,7	17,5	13,75	0,6	0,6	1,7	0,9	4,2	1,9	1,1
40	**272**	213,6	18,69	21,67	0,7	4,8	8,7	1,3	7,4	3,1	1,2
39	**269,4**	135,9	7,364	19,24	0,9	1,2	19,9	1,7	8,9	1,5	1,2
38	**263,5**	228,3	17,73	8,032	0,6	3,1	25,8	1,5	9,6	4,8	1,6
37	**261**	145,7	8,907	18,1	1,1	1,8	17,5	1,6	9,2	1,5	1,1
36	**252,1**	246,2	18,91	16,23	0,7	0,6	7,1	1	5,7	2,4	1,5
35	**235,6**	226,9	17,02	17,36	0,7	0,6	7,7	1,5	4,2	2,4	1
34	**232,6**	413,4	5,623	8,077	0,3	0,4	2,5	0,8	3,3	1,7	1,1
33	**217,6**	108,4	1	11,09	0,7	1,2	18,5	1,6	7,4	2,1	1,2
32	**198**	241,8	18,78	13,24	1	1,2	20,2	1,8	10,3	3,6	1,8
31	**197,2**	138,9	1	12,86	0,9	0,9	16,1	2,1	9	2,2	1,8
30	**182,2**	180,6	9,825	5,606	0,3	0,3	0,7	1,5	4,2	1,8	0,7
29	**173,2**	286,8	15,92	9,697	0,9	0,8	11,5	1,6	3	4,1	1,9
28	**161**	289,2	21,57	19,11	1,4	0,5	16,4	2	7,2	4,7	0,8
27	**158**	233,6	5,142	10,02	0,8	1,3	14,7	1,9	6,6	2,1	1,4
26	**157**	439,9	1	7,577	0,3	0,3	2,4	0,9	2,5	1,6	0,8
25	**130,6**	340,6	19,91	14,69	2	1,3	34,9	2,4	7,3	5,8	1,1
24	**120,9**	350,7	24,68	16,06	1,3	0,5	31,1	2	11,3	6,9	2
23	**120,1**	331	21,34	6,901	0,4	0,3	1,2	0,9	2,6	1,8	0,8
22	**112,6**	399,2	11,72	24,08	0,5	0,3	1,1	0,8	10,6	2,7	1
21	**110,1**	353,6	13,12	23,74	1,5	0,4	14,9	2	9	5,6	1,7
20	**102,6**	279,3	19,16	23,14	2,1	4,3	26,5	3,1	5,2	10,9	0,5
19	**92,1**	405,6	10,14	7,376	0,5	0,3	1,1	1,1	2,8	1,6	0,6
18	**85,8**	317,7	25,22	21,57	3,4	2,8	64,7	3,9	9,5	7,7	1,6
17	**75,3**	605,9	9,789	34,41	2,2	0,5	24,2	3	10,9	8	1,3

16	**73,9**	307,6	22,57	39,48	3,5	1,1	70,4	4,7	5,9	7,9	1,1
14	**55,9**	304,9	23,56	35,41	1,6	0,6	41,2	3,6	8,4	6,2	1,5
13	**45,9**	319,6	19,73	27,57	1,4	0,4	15,3	2,7	4,1	3,4	1,3
12	**33,2**	313,4	34,62	29,64	4	0,7	97,4	5,6	11,5	12,8	1,2
11	**24,9**	351,3	27,49	25,84	2,2	0,5	33,1	2,5	14,7	6,6	1,4
10	**17,4**	469,3	27,69	28,16	2,2	0,5	89,9	3,7	12,4	6,7	1,8
9	**15,1**	677,5	31,04	21,69	3,7	0,3	37,2	3,1	8,4	10,5	1,3
8	**13,6**	317,8	32,32	29,38	2,4	0,5	19,4	2,7	10	7,9	2
7	**12,4**	265,7	21,21	41,41	3,1	1,6	35,8	4,2	16,3	12,3	2,6
6	**11,6**	168,8	17,53	32,19	2,6	2,8	54,8	3,1	12,6	7,9	2,5
5	**6,7**	244,4	32,35	13,68	3,6	0,9	31,2	2,9	7,5	10,9	1,6
4	**5,5**	97,1	15,35	25,92	3	0,7	26,5	4,1	18	9,2	4,9
3	**4**	224,3	46,26	20,43	5,3	10	42	3,8	11,8	9,3	6
2	**2**	85,96	1	5,19	0,4	5,1	6,2	3,7	22,5	1,8	5,6
1	**0,3**	331,7	62,12	109,5	9,3	244,7	235,4	9,9	74,9	16,3	296,3

Section 4

Sample Name	Thickness (m)	Ba (ppm)	Cu (ppm)	Ni (ppm)	V EF	Zn EF	Mo EF	U EF	As EF	Sb EF	Pb EF
40	**230**	464,8	< L.D.	13,91	0,9	1,6	20	1,4	7,3	1	1
39	**212**	5940	6,703	7,989	0,3	0,3	0,8	0,7	2,8	1,6	1
38	**185**	273	16,23	14,2	1,1	8,5	23,1	1,5	6,6	4,2	1,3
37	**172**	263,8	16,09	17,26	1,2	0,7	10,2	1,9	8	2,9	1,3
36	**168**	121,4	6,594	10,49	0,9	1,5	6	1,4	5,2	1	1,2
35	**156**	180,7	30,48	8,112	0,5	0,4	1,9	1,9	11,6	1	1,1
34	**148**	274,3	25,05	12,62	1,7	3,3	20,8	2	8,2	4	0,8
33	**143**	321,2	26,72	18,86	1,3	2,3	31,8	2,4	11,4	4	1,5
32	**137**	275,9	13,72	44,63	1,2	0,9	22,7	2,4	10,2	3,5	1,3
31	**132**	147,6	11,61	33,59	1,9	0,7	33,2	3	7,3	4,1	1,1
30	**119**	419,6	6,129	16,9	0,3	0,2	3,7	0,8	3,6	2,2	0,9
29	**126**	346,9	30,69	12,53	1,7	0,4	18	2	6	4,7	0,9
28	**122**	323,7	18,31	26,32	1,5	3,1	45,4	2,1	8,6	4,1	1
27	**119**	338,5	14,46	27,67	1,7	1,3	26	1,8	9,9	7,2	1,2

26	**115**	335,8	21,06	50,8	1,5	3,8	15,8	1,8	6,8	4,7	1,2
25	**109**	347,4	15,84	21,26	1,2	0,6	20,1	1,6	7,4	4,2	1,4
24	**99**	379,7	8,841	10,54	0,5	0,3	0,9	1	3,4	1,6	1
23	**93**	149,5	11,83	33,76	1,9	0,9	20,3	2,1	20,6	5,8	2
22	**88**	323,8	55,64	15,55	1,4	0,4	12,7	1,8	5,5	3,8	2,1
21	**80**	188,1	6,552	56,24	2,3	18,7	138,4	4,3	9,6	6,8	1,3
20	**75**	1103	8,718	13,65	0,5	0,4	1,8	1	2,5	1,9	0,6
19	**70**	408,4	11,21	10,96	0,6	0,3	1,6	0,9	3,5	1,9	1
18	**67**	318,3	23,92	18,51	2,8	5	29,1	3	7,9	5,7	2,3
17	**63**	309,2	23,04	27,47	1,8	1	18	3,1	4,5	4,7	1,1
16	**60**	402,8	19,39	32,88	3	0,6	43,4	3,3	12,4	7	1,3
15	**53**	392,8	25,3	25,67	2	0,6	47,8	2,8	9,2	7,2	1
14	**49**	447,8	28,98	45,94	2,7	2,2	135,1	3,4	9,1	7,8	1,5
13	**47**	320	19,98	38,14	2,4	1,2	32,9	2,7	7,3	8,3	1,3
12	**31**	322,5	39,97	53,19	1,9	0,6	24,5	3,1	7,8	5,4	1,1
11	**26**	331,7	29,87	67,51	2,3	0,4	57,4	3,4	8,7	5,7	1,6
10	**22**	303,8	34,35	49,82	4,6	0,7	86,2	3,7	13,1	13,6	1,3
9	**20**	335,5	30,25	53,75	2,4	0,4	48,3	3,2	9,7	4,7	1,5
8	**18**	325,7	22,36	23,83	3,7	0,5	98,8	4,6	7,1	8,8	1,6
7	**15**	391,1	24,53	60,29	2,8	2,9	69,1	2,8	8,2	7	1,1
6	**12**	799	20,79	47,24	2,2	0,4	34,8	3	10,2	5,3	1
5	**10**	321,1	29,83	62,73	2,5	1,5	75,6	3	14,4	7,3	3,9
4	**8**	1257	15,94	48,76	2,4	1,6	41,8	2,5	10,3	7,1	3,2
3	**6**	930,7	24,88	27,28	2,6	0,4	22,9	3,3	8,3	8,7	3,4
2	**3**	507,2	19,79	49,64	2,9	1,7	33,3	2,6	18,1	9,5	4,5
1	**1**	172,6	15,32	27,41	1,5	3,8	10,1	2,3	12,1	4,8	3,7

Section 5

Sample Name	Thickness (m)	Ba (ppm)	Cu (ppm)	Ni (ppm)	V EF	Zn EF	Mo EF	U EF	As EF	Sb EF	Pb EF
42	**248**	297,7	16,16	23,28	0,6	1	6,5	1,1	5,6	2,1	1,1
41	**242**	259,9	15,96	26,75	0,6	0,9	2,4	1	4	1,7	1,1
40	**230**	282,9	12,49	26,75	0,7	0,5	2,9	1	4,3	2	1,2

38	**208**	234,6	15,83	46,1	0,8	0,6	6,6	1,4	6,1	2,3	1,1
37	**191**	1182	8,224	13,78	0,5	0,6	2	1,1	4,1	1,8	0,9
36	**185**	192,9	13,65	22,12	0,6	0,6	3	1,2	4,9	2	1
35	**156**	206,5	14,3	11,07	0,9	0,6	7,8	1,7	4,6	2,3	0,6
34	**138**	392,1	15,65	29,4	1,1	0,8	15	2,5	3,6	3,1	0,8
33	**133**	299,8	19,76	19,33	1,3	0,5	8,7	2	4,4	3,4	1
32	**130**	384,6	8,8	16,61	0,6	0,6	9,3	1,3	3,4	2,9	0,9
31	**126**	298	11,37	21,58	1,7	0,9	40,2	2,2	7	5,8	0,6
30	**124**	449,9	19,07	24,01	1,4	4,4	34	1,9	5,1	4	1,1
29	**119**	409,7	16,3	24,89	1,1	0,5	16,3	1,5	7,3	4,4	0,7
28	**115**	338,7	21,04	24,64	1,1	0,5	21,8	1,8	6,2	4,2	0,5
27	**113**	554,5	20,32	40,22	1,8	2,9	29,7	1,9	7,5	8,5	0,7
26	**109**	612,7	52,99	18,54	1,5	1,2	16,9	2	9,4	5	0,7
25	**107**	769	12,42	30,61	0,9	0,9	18,8	2	6,6	4,2	1
24	**104**	392,6	12,87	35,68	1,6	1,3	29,8	1,8	13,1	6,9	1,7
23	**78**	298,4	8,129	9,225	0,4	0,3	0	0,9	4,3	1,5	0,6
22	**76**	163,1	11,54	48,51	1,9	1,6	35,1	2,3	11,9	5,3	1,7
21	**74**	305,7	10,21	8,162	0,5	0,4	1	0,8	2,5	1,7	0,6
20	**70**	330,5	17,21	30,99	1,8	1,1	24,4	2,4	7,4	5,2	1,1
19	**68**	415,4	14,89	31,61	2,2	0,4	60,6	2,5	7,1	5,6	0,7
18	**64**	308,5	26,23	47,26	1,7	0,4	21,4	3,4	5,8	4,4	0,6
17	**60**	327,9	12,35	42,78	3,3	4,2	90,4	4,1	12,1	8,3	1,3
16	**58**	302,1	17,22	36,53	1,6	0,4	39,6	2,4	7,8	4,7	1,1
15	**55**	326,2	21,35	14,52	2,3	0,4	21,5	3,6	7,7	4,2	0,7
14	**53**	277,7	22,46	20,26	2,5	0,6	31,8	3,2	12	6,9	1,1
13	**50**	614,1	23,18	35,11	1,3	0,4	13,8	2,3	3,3	3,3	0,9
12	**46**	302	52,18	69,44	3,9	2,3	40,6	4,7	10,9	9,5	1,2
11	**42**	1918	21,95	30,48	1,3	0,4	19,3	2,1	3,9	3,7	1
10	**38**	308,8	24,63	41,94	2,4	0,5	27	2,3	9,7	7,2	1,1
9	**35**	556,3	26,69	28,71	2,2	0,4	20,8	2,6	5,7	6,7	0,7
8	31	475,9	18,47	42,52	2,4	0,5	40	1,9	8,7	6,1	1
7	28	473,9	22,63	27,96	1,5	0,4	30,7	2,2	7	6,4	0,9
6	24	1034	30,06	56,61	2,2	0,4	24	2,6	9,2	5,3	0,9
5	20	525	33,12	37,18	2,4	0,3	48,5	2,9	8,9	7	2,4
4	18	529,5	40,18	63,24	2,5	7,2	48,6	4,1	13	5,8	2,9

3	16	2094	17,16	35,56	1,8	0,4	19,6	2,1	5,3	4,3	1,3
2	14	1078	27,63	23,97	1,4	1	8,4	2	14,1	6,8	4,2
1	2	242,2	109,1	35,6	7,3	9	109,8	9,9	10,7	16,3	35,7

Covunco Section

Sample Name	Thickness (m)	Ba (ppm)	Cu (ppm)	Ni (ppm)	V EF	Zn EF	Mo EF	U EF	As EF	Sb EF	Pb EF
38	**330**	217,8	17	15,8	0,6	0,4	0,4	1			0,8
37	**325**	284,9	20,8	20,9	0,8	2,2	2	1,5	27,2	3,4	2,1
36	**322**	271,7	27,2	19,7	0,8	1,2	0,6	1,4	1,8	1,3	1,2
35	**304**	215,5	14,7	7,4	0,5	0,4	0,4	1,1	2,4		0,8
34	**299**	1045	17,5	21,4	0,6	0,3	0,4	1,1	1,5		0,9
33	**296**	232,6	20,3	31,1	1	8,8	3,7	1,2	7,3	2,7	1
32	**293**	243,3	20,5	15,5	0,6	0,5	0,7	0,8	4,1	1,5	0,6
31	**263**	368,8	14,4	14,7	0,7	1,2	2,1	1,8	9,3	2,9	1,2
30	**260**	222,3	29,3	18,1	0,8	28	2,4	1,5	8,2	3	1,2
29	**253**	221,5	12	8,1	0,5	0,3	0,6	1,4	/	/	0,4
28	**245**	317,3	13,9	14,9	0,5	0,4	0,8	1,1	4,4	2,7	1
27	**240**	277,8	15,6	13,7	0,5	0,4	1	0,9	5,7	2,2	0,9
26	**218**	143	12,9	13,6	0,6	0,5	1,8	2,1	7	2,5	1,1
25	**214**	265,5	21,2	35,9	1,3	3	1,8	2,4	7,5	3,2	0,9
24	**207**	212,9	28,9	25,1	1	0,5	7,8	1,6	7,6	3,3	1
23	**204**	45,5	7,4	10,9	1	0,7	8,9	3	7,1	/	1,1
22	**200**	340,3	19,8	27,1	1,6	11,5	15,3	4,1	14,4	5,1	1,3
21	**167**	51,6	6,3	9,6	1,1	/	4,7	3,2	8,3	/	1,1
20	**161**	79,2	6,3	18,4	1	3,5	4,6	5,2	18,2	/	1,5
19	**120**	84,5	6	13,6	1,5	/	5,8	4,8	15,3	/	1,8
18	**118**	618	8,8	22,7	2,1	1,3	30,1	3,9	17,9	5,5	1,5
17	**115**	292,5	18,2	28	1,5	0,4	6,5	3,7	12,6	4,8	1,4
16	**113**	1036	11,1	7,4	0,3	0,8	3,3	0,5	4,2	3,4	1
15	**100**	198,2	11,8	23,2	1	0,6	12,7	6,2	12,1	4,9	1,3

14	***91***	*781,1*	*19,5*	*45,7*	*1,7*	*0,6*	*22,3*	*2,8*	*12,5*	*7,2*	*1,3*
13	***86***	*174,1*	*20,8*	*116,2*	*4,2*	*1,2*	*90,3*	*3,5*	*25,1*	*10,2*	*1,3*
12	***84***	*168*	*17,4*	*43,2*	*1,3*	*0,7*	*30*	*3,5*	*8,5*	*2,7*	*1,2*
11	***81***	*148,2*	*16,3*	*19,7*	*0,7*	*0,5*	*26,1*	*1,2*	*13,9*	*3,2*	*1*
10	***75***	*210,4*	*28,1*	*78,8*	*2,3*	*0,5*	*81,2*	*3*	*12,7*	*4,6*	*1,2*
9	***69***	*179,1*	*30,2*	*87,7*	*3,8*	*1*	*77,9*	*5,3*	*17,8*	*9,9*	*1,3*
8	***66***	*285,8*	*41,4*	*111,5*	*7,4*	*2,7*	*107,4*	*6,4*	*20,4*	*13,8*	*1,4*
7	***62***	*278,6*	*33,2*	*110,8*	*3,6*	*0,4*	*71,3*	*2,6*	*11,4*	*10,2*	*1,3*
6	***41***	*248,9*	*34,5*	*112,4*	*4,8*	*3,1*	*83,3*	*5,6*	*14,7*	*9,8*	*1,4*
5	***21***	*343,7*	*22,3*	*21,7*	*0,7*	*0,3*	*3,2*	*0,9*	*4,3*	*2,4*	*0,7*
4	***18***	*410,3*	*13,1*	*9,3*	*0,4*	*0,3*	*4,2*	*0,8*	*7,8*	*2,7*	*1,2*
3	***15***	*308,6*	*23,5*	*17,1*	*0,8*	*0,4*	*5,6*	*1*	*9,9*	*3,1*	*1,5*
2	***5***	*122,6*	*12,9*	*41*	*1,8*	*9,9*	*7,7*	*4*	*33,4*	*7,2*	*4,1*
1	***1***	*593,5*	*23,2*	*39,1*	*4,1*	*154*	*27,7*	*7,4*	*62,6*	*9,1*	*13,6*

Appendix 2. Rock-Eval pyrolysis data

TOC: Total Organic Carbon, wt%

S1- volatile hydrocarbon (HC) content, mg HC/g rock

S2- remaining HC generative potential, mg HC/g rock

S3- carbon dioxide content, mg CO_2/g rock

HI- Hydrogen Index = S2 X 100/ TOC, mg HC/g TOC

OI- Oxygen Index = S3 X 100/ TOC, mg CO_2/g TOC

PI- Production Index = S1/ (S1+S2)

Section 1

Sample Name	Thickness (m)	TOC	S1	S2	S3	IH	IO	PI	TMAx
48	210	3,38	0,16	14,54	0,42	430	12	0,01	414
47	200	1,47	0,04	1,62	1,35	110	92	0,02	418
46	197	0,85	0,03	1,59	0,79	187	93	0,02	434
45	194	0,79	0,02	0,34	1,65	43	209	0,06	432
44	190	0,79	0,02	0,39	1,1	49	139	0,05	432
43	186	0,68	0,02	0,35	1,46	51	215	0,05	433
42	182	0,99	0,03	0,99	1,17	100	118	0,03	429
41	176	1,3	0,03	1,75	1,39	135	107	0,02	433
40	172	1,08	0,02	0,99	1,43	92	132	0,02	438
39	159	0,01	0	0,02	0,25	200	2500	0	444
38	157	0,54	0,01	0,27	0,77	50	143	0,04	430
37	152	2,56	0,04	2,54	4,57	99	179	0,02	430
36	147	0,92	0,02	0,82	1,55	89	168	0,02	434
34	143	0,62	0,02	0,34	0,98	55	158	0,06	429
33	139	1,21	0,02	1,23	1,9	102	157	0,02	435
32	133	0,56	0,02	0,41	0,58	73	104	0,05	427
31	130	2,74	0,07	6,42	2,28	234	83	0,01	423
30	125	0,02	0	0,02	0,17	100	850	0	444
29	120	0,5	0,01	0,03	0,48	6	96	0,25	499

28	**110**	0,07	0	0,03	0,19	43	271	0	323
27	**103**	0,09	0	0,02	0,6	22	667	0	508
26	**77**	3,56	0,08	5,41	3,57	152	100	0,01	434
25	**68**	1,68	0,03	1,15	2,47	68	147	0,03	429
24	**66**	2,02	0,03	1,78	3,13	88	155	0,02	435
23	**64**	0,86	0,01	0,45	1,84	52	214	0,02	434
22	**60**	7,93	0,95	32,82	5,69	414	72	0,03	409
21	**58**	2,61	0,05	4,82	2,99	185	115	0,01	428
20	**55**	3,99	0,15	9,74	4,59	244	115	0,02	418
19	**53**	0,62	0,02	0,37	0,71	60	115	0,05	432
18	**51**	6,83	1,04	36,87	3,08	540	45	0,03	416
17	**50**	2,46	0,08	8,11	1,56	330	63	0,01	421
15	**45**	0,9	0,01	0,52	1,92	58	213	0,02	436
14	**42**	1,19	0,02	0,9	2,78	76	234	0,02	436
13	**40**	1,87	0,03	2,25	3,77	120	202	0,01	431
12	**29**	9,16	2,05	54,25	2,41	592	26	0,04	417
11	**27**	0,46	0,01	0,69	0,86	150	187	0,01	440
10	**25**	0,44	0,01	0,71	0,82	161	186	0,01	440
9	**22**	9,8	2,5	62,23	1,38	635	14	0,04	416
8	**20**	1,36	0,03	1,07	2,07	79	152	0,03	428
7	**18**	5,13	1,1	25,76	2,39	502	47	0,04	413
6	**16**	2,26	0,13	3,45	2,78	153	123	0,04	423
5	**14**	1,93	0,03	1,94	3,95	101	205	0,02	431
4	**11**	1,76	0,04	1,82	2,88	103	164	0,02	431
3	**9**	2,84	0,17	8,45	1,81	298	64	0,02	421
2	**7**	0,23	0,01	0,21	0,56	91	243	0,05	439
1	**1**	21,05	3,29	118,7	9	564	43	0,03	415

Section 2

Sample Name	Thickness (m)	TOC	S1	S2	S3	IH	IO	PI	TMAx
32	**243**	0,03	0	0,02	0,11	67	367	0	375

31	***237***	*0,03*	*0*	*0,03*	*0,24*	*100*	*800*	*0*	*412*
30	***232***	*0,04*	*0*	*0,03*	*0,36*	*75*	*900*	*0*	*603*
29	***227***	*0,05*	*0*	*0,01*	*0,31*	*20*	*620*	*0*	*404*
28	***202***	*0,67*	*0,02*	*0,36*	*1,08*	*54*	*161*	*0,05*	*428*
27	***198***	*0,45*	*0,01*	*0,17*	*0,72*	*38*	*160*	*0,06*	*434*
26	***190***	*0,2*	*0,01*	*0,32*	*0,52*	*160*	*260*	*0,03*	*438*
25	***179***	*1,67*	*0,03*	*2,34*	*2,65*	*140*	*159*	*0,01*	*433*
24	***170***	*1,16*	*0,07*	*4,53*	*0,52*	*391*	*45*	*0,02*	*419*
23	***168***	*0,04*	*0*	*0,01*	*0,75*	*25*	*1875*	*0*	*432*
22bis	***166***	*0*	*0*	*0,02*	*0,06*	*<0*	*<0*	*0*	*361*
22	***162***	*0,03*	*0*	*0,01*	*0,17*	*33*	*567*	*0*	*392*
21	***157***	*1,06*	*0,02*	*0,93*	*1,43*	*88*	*135*	*0,02*	*426*
20	***140***	*0,03*	*0*	*0,03*	*0,2*	*100*	*667*	*0*	*495*
19	***131***	*0,06*	*0*	*0,04*	*0,42*	*67*	*700*	*0*	*338*
18	***113***	*1,87*	*0,03*	*2,71*	*2,55*	*145*	*136*	*0,01*	*434*
17	***107***	*0,28*	*0,01*	*0,05*	*0,73*	*18*	*261*	*0,17*	*431*
16	***95***	*0,65*	*0,01*	*0,25*	*1,33*	*38*	*205*	*0,04*	*430*
15	***92***	*0,04*	*0*	*0,01*	*0,4*	*25*	*1000*	*0*	*395*
14	***90***	*0,06*	*0,01*	*0,01*	*0,13*	*17*	*217*	*0,5*	*395*
13	***86***	*0,04*	*0*	*0,02*	*0,55*	*50*	*1375*	*0*	*495*
12	***80***	*0,01*	*0*	*0,01*	*0,07*	*100*	*700*	*0*	*494*
11	***69***	*0,03*	*0*	*0,03*	*0,16*	*100*	*533*	*0*	*341*
10	***50***	*0,51*	*0,01*	*0,1*	*1,57*	*20*	*308*	*0,09*	*483*
9	***40***	*0,02*	*0,01*	*0,02*	*0,15*	*100*	*750*	*0,33*	*473*
8	***37***	*0,03*	*0*	*0*	*0,45*	*0*	*1500*	*<0.00*	*495*
7	***34***	*0,01*	*0*	*0,01*	*0,19*	*100*	*1900*	*0*	*388*
6	***30***	*0,01*	*0,01*	*0,01*	*0,04*	*100*	*400*	*0,5*	*404*
5	***27***	*0,04*	*0*	*0,02*	*0,57*	*50*	*1425*	*0*	*494*
4	***22***	*0,04*	*0*	*0,02*	*0,51*	*50*	*1275*	*0*	*497*
3	***20***	*0,03*	*0*	*0,03*	*0,37*	*100*	*1233*	*0*	*589*
2	***8***	*0,03*	*0*	*0,02*	*0,45*	*67*	*1500*	*0*	*376*
1	***0***	*0,04*	*0*	*0,03*	*0,52*	*75*	*1300*	*0*	*492*

Section 3

Sample Name	Thickness (m)	TOC	S1	S2	S3	IH	IO	PI	TMAx
59	**443**	0,05	0,01	0,07	0,25	140	500	0,13	372
58	**427**	0,04	0,01	0,04	0,19	100	475	0,2	339
57	**421**	0,05	0,01	0,04	0,25	80	500	0,2	421
56	**410**	0,06	0,01	0,07	0,24	117	400	0,13	427
55	**406**	0,05	0,01	0,05	0,27	100	540	0,17	427
54	**397**	0,02	0,01	0,03	0,2	150	1000	0,25	410
53	**390**	0,01	0,02	0,03	0,21	300	2100	0,4	381
52	**384**	0,02	0,01	0,02	0,19	100	950	0,33	407
51	**374**	0,05	0,01	0,04	0,22	80	440	0,2	423
50	**373**	0,02	0,01	0,02	0,16	100	800	0,33	397
49	**366,7**	0,01	0,01	0,02	0,16	200	1600	0,33	408
48	**361,5**	0,05	0,01	0,04	0,22	80	440	0,2	424
47	**360**	0,04	0,01	0,04	0,18	100	450	0,2	424
46	**351**	0,06	0,01	0,03	0,17	50	283	0,25	428
45	**340**	0,08	0,01	0,02	0,26	25	325	0,33	435
44	**330**	0,03	0,02	0,02	0,2	67	667	0,5	424
43	**320,5**	0,04	0,03	0,03	0,2	75	500	0,5	427
42	**310**	0,05	0,03	0,02	0,16	40	320	0,6	525
41	**300**	0,16	0,02	0,05	0,28	31	175	0,29	430
40	**272**	0,12	0,02	0,03	0,25	25	208	0,4	427
39	**269,4**	0,07	0,02	0,04	0,36	57	514	0,33	440
38	**263,5**	0,08	0,03	0,02	0,36	25	450	0,6	421
37	**261**	0,08	0,02	0,07	0,41	88	513	0,22	437
36	**252,1**	0,23	0,03	0,05	0,35	22	152	0,38	432
35	**235,6**	0,32	0,04	0,07	0,56	22	175	0,36	506
34	**232,6**	0,01	0,01	0,02	0,21	200	2100	0,33	493
33	**217,6**	0,08	0,01	0,04	0,4	50	500	0,2	439
32	**198**	0,55	0,07	0,2	1,25	36	227	0,26	436
31	**197,2**	0,04	0,01	0,04	0,33	100	825	0,2	441
30	**182,2**	0,1	0,04	0,03	0,23	30	230	0,57	418
29	**173,2**	0,52	0,04	0,45	0,55	87	106	0,08	433

28	**161**	*0,49*	*0,02*	*0,14*	*1,02*	*29*	*208*	*0,13*	*485*
27	**158**	*0,07*	*0,01*	*0,1*	*0,64*	*143*	*914*	*0,09*	*449*
26	**157**	*0,01*	*0,01*	*0,02*	*0,21*	*200*	*2100*	*0,33*	*392*
25	**130,6**	*0,39*	*0,02*	*0,14*	*0,86*	*36*	*221*	*0,13*	*430*
24	**120,9**	*0,56*	*0,02*	*0,3*	*1,1*	*54*	*196*	*0,06*	*437*
23	**120,1**	*0,02*	*0,01*	*0,03*	*0,18*	*150*	*900*	*0,25*	*406*
22	**112,6**	*0,03*	*0,01*	*0,04*	*0,23*	*133*	*767*	*0,2*	*454*
21	**110,1**	*2,17*	*0,05*	*5,27*	*0,96*	*243*	*44*	*0,01*	*421*
20	**102,6**	*2,12*	*0,09*	*5,18*	*2,1*	*244*	*99*	*0,02*	*432*
19	**92,1**	*0,03*	*0,01*	*0,04*	*0,16*	*133*	*533*	*0,2*	*424*
18	**85,8**	*3,26*	*0,08*	*6,03*	*3,67*	*185*	*113*	*0,01*	*426*
17	**75,3**	*0,42*	*0,03*	*0,76*	*0,45*	*181*	*107*	*0,04*	*433*
16	**73,9**	*6,16*	*0,15*	*15,98*	*5,69*	*259*	*92*	*0,01*	*420*
15	**58,9**	*0,11*	*0,02*	*0,31*	*0,24*	*282*	*218*	*0,06*	*427*
14	**55,9**	*1,44*	*0,04*	*1,39*	*2,05*	*97*	*142*	*0,03*	*432*
13	**45,9**	*1,25*	*0,03*	*1,16*	*1,64*	*93*	*131*	*0,03*	*434*
12	**33,2**	*5,6*	*0,23*	*17,78*	*4,79*	*318*	*86*	*0,01*	*418*
11	**24,9**	*1,21*	*0,04*	*1,09*	*1,73*	*90*	*143*	*0,04*	*428*
10	**17,4**	*3,18*	*0,15*	*7,25*	*3,55*	*228*	*112*	*0,02*	*424*
9	**15,1**	*4,38*	*0,3*	*17,2*	*2,91*	*393*	*66*	*0,02*	*416*
8	**13,6**	*1,83*	*0,06*	*2,5*	*2,25*	*137*	*123*	*0,02*	*428*
7	**12,4**	*0,25*	*0,03*	*0,37*	*0,77*	*148*	*308*	*0,08*	*440*
6	**11,6**	*0,98*	*0,08*	*2,68*	*0,77*	*273*	*79*	*0,03*	*435*
5	**6,7**	*5,69*	*0,43*	*23,63*	*3,87*	*415*	*68*	*0,02*	*420*
4	**5,5**	*0,08*	*0,01*	*0,1*	*0,52*	*125*	*650*	*0,09*	*443*
3	**4**	*7,67*	*0,55*	*41,37*	*3,33*	*539*	*43*	*0,01*	*415*
2	**2**	*0,04*	*0,01*	*0,03*	*0,3*	*75*	*750*	*0,25*	*425*
1	**0,3**	*24,53*	*4,89*	*123*	*11,79*	*501*	*48*	*0,04*	*409*

Section 4

Sample Name	*Thickness (m)*	*TOC*	*S1*	*S2*	*S3*	*IH*	*IO*	*PI*	*TMAx*

40	**230**	0,03	0	0,02	0,34	67	1133	0	598
39	**212**	0,01	0	0,02	0,18	200	1800	0	419
38	**185**	1,44	0,03	2,42	1,07	168	74	0,01	428
37	**172**	1,67	0,04	2,44	1,28	146	77	0,02	428
36	**168**	0,22	0,01	0,33	0,35	150	159	0,03	435
35	**156**	0,02	0	0,02	0,26	100	1300	0	498
34	**148**	0,21	0,01	0,07	0,64	33	305	0,13	429
33	**143**	0,51	0,01	0,25	1,26	49	247	0,04	438
32	**137**	3,96	0,35	20,49	0,49	517	12	0,02	415
31	**132**	2,01	0,06	7,76	0,92	386	46	0,01	426
30	**119**	0,02	0	0,05	0,27	250	1350	0	443
29	**126**	1,03	0,01	0,81	1,82	79	177	0,01	438
28	**122**	2,46	0,08	5,62	1,02	228	41	0,01	415
27	**119**	2,23	0,06	6,25	1,21	280	54	0,01	421
26	**115**	2,01	0,15	4,94	0,98	246	49	0,03	417
25	**109**	1,25	0,03	1,66	0,9	133	72	0,02	424
24	**99**	0,01	0	0,02	0,15	200	1500	0	470
23	**93**	0,03	0	0,02	0,44	67	1467	0	452
22	**88**	0,21	0,01	0,05	0,7	24	333	0,17	464
21	**80**	0,03	0	0,01	0,53	33	1767	0	499
20	**75**	0,03	0	0,01	0,17	33	567	0	408
19	**70**	0,03	0	0,01	0,16	33	533	0	458
18	**67**	0,52	0,01	0,11	1,28	21	246	0,08	420
17	**63**	1,84	0,04	3,53	1,95	192	106	0,01	436
16	**60**	1,06	0,02	0,51	2,36	48	223	0,04	438
15	**53**	4,31	0,29	15,13	3,46	351	80	0,02	413
14	**49**	6,63	0,31	27,83	3,93	420	59	0,01	415
13	**47**	3,16	0,13	11,82	1,84	374	58	0,01	419
12	**31**	2,61	0,09	5,96	2,35	228	90	0,01	428
11	**26**	1,24	0,04	1,26	2,04	102	165	0,03	429
10	**22**	8,45	1,4	51,26	1,89	607	22	0,03	418
9	**20**	1,87	0,09	2	2,84	107	152	0,04	423
8	**18**	4,7	0,31	12,39	4,86	264	103	0,02	424

7	**15**	5,15	1,11	27,19	1,6	528	31	0,04	413
6	**12**	2,82	0,11	6,48	2,64	230	94	0,02	425
5	**10**	2,91	0,06	5,38	4,06	185	140	0,01	430
4	**8**	0,05	0	0,03	0,53	60	1060	0	451
3	**6**	2,35	0,07	4,21	2,61	179	111	0,02	427
2	**3**	0,07	0	0,06	0,51	86	729	0	442
1	**1**	0,19	0	0,24	0,57	126	300	0	442

Section 5

Sample Name	Thickness (m)	TOC	S1	S2	S3	IH	IO	PI	TMAx
42	**248**	0,71	0,01	0,6	0,67	85	94	0,02	436
41	**242**	1,02	0,02	1,16	0,67	114	66	0,02	436
40	**230**	0,68	0,03	1,22	0,18	179	26	0,02	422
39	**220**	1,04	0,05	2,21	0,11	213	11	0,02	413
38	**208**	1,64	0,06	4,19	0,51	255	31	0,01	425
37	**191**	0,5	0,02	0,95	0,2	190	40	0,02	425
36	**185**	0,81	0,04	1,99	0,24	246	30	0,02	425
35	**156**	1,86	0,04	3,36	0,83	181	45	0,01	419
34	**138**	2,52	0,06	5,98	2,25	237	89	0,01	431
33	**133**	0,98	0,03	0,83	1,24	85	127	0,03	429
32	**130**	0,26	0,01	0,11	0,39	42	150	0,08	430
31	**126**	4,38	0,13	17,43	2,27	398	52	0,01	414
30	**124**	2,15	0,05	5,16	1,57	240	73	0,01	427
29	**119**	1,15	0,02	1,95	0,79	170	69	0,01	427
28	**115**	0,46	0,01	0,3	0,66	65	143	0,03	433
27	**113**	1,94	0,05	4,4	1,4	227	72	0,01	423
26	**109**	0,88	0,02	0,82	1,34	93	152	0,02	435
25	**107**	1,62	0,04	3,44	1,15	212	71	0,01	427
24	**104**	1,86	0,04	4,65	1,2	250	65	0,01	422
23	**78**	0,05	0,01	0,07	0,26	140	520	0,13	339
22	**76**	0,02	0	0,01	0,33	50	1650	0	494

21	**74**	0,03	0	0,04	0,15	133	500	0	468
20	**70**	1,4	0,03	2,29	1,33	164	95	0,01	432
19	**68**	5,69	0,22	28,49	1,53	501	27	0,01	414
18	**64**	2,91	0,04	4,92	3,22	169	111	0,01	433
17	**60**	8,4	0,46	41,67	3,42	496	41	0,01	413
16	**58**	2,63	0,09	6,97	1,83	265	70	0,01	421
15	**55**	0,87	0,01	0,32	1,96	37	225	0,03	422
14	**53**	0,5	0,01	0,17	1,46	34	292	0,06	420
13	**50**	1,01	0,02	0,87	1,12	86	111	0,02	434
12	**46**	3,37	0,06	6,63	3,6	197	107	0,01	433
11	**42**	0,9	0,02	0,81	1,23	90	137	0,02	430
10	**38**	0,99	0,02	0,74	1,57	75	159	0,03	427
9	**35**	1,43	0,03	2,17	1,72	152	120	0,01	435
8	**31**	3,78	0,44	14,66	2,24	388	59	0,03	414
7	**28**	2,6	0,07	6,96	2,27	268	87	0,01	424
6	**24**	2,6	0,08	6,61	2,32	254	89	0,01	426
5	**20**	3,48	0,13	10,29	3,08	296	89	0,01	423
4	**18**	4,86	0,07	8,08	6,19	166	127	0,01	430
3	**16**	1,88	0,04	3,84	1,76	204	94	0,01	431
2	**14**	2,52	0,07	6,57	2,24	261	89	0,01	423
1	**2**	20,41	1,78	66,86	18,03	328	88	0,03	419

Covunco Section

Sample Name	Thickness (m)	TOC	S1	S2	S3	IH	IO	PI	TMAx
38	**330**	0,12	0,00	0,06	0,57	50	475	0,00	494
37	**325**	0,08	0,00	0,09	0,49	113	613	0,00	452
36	**322**	0,12	0,01	0,05	0,44	42	367	0,17	450
35	**304**	0,04	0,00	0,02	0,19	50	475	0,00	439
34	**299**	0,03	0,00	0,01	0,35	33	1167	0,00	460
33	**296**	0,26	0,01	0,04	0,41	15	158	0,20	436
32	**293**	0,14	0,00	0,06	0,48	43	343	0,00	439

31	***263***	*0,32*	*0,01*	*0,25*	*0,69*	*78*	*216*	*0,04*	*441*
30	***260***	*0,18*	*0,01*	*0,12*	*0,60*	*67*	*333*	*0,08*	*443*
29	***253***	*0,2*	*0,01*	*0,16*	*0,57*	*80*	*285*	*0,06*	*444*
28	***245***	*0,03*	*0,00*	*0,02*	*0,26*	*67*	*867*	*0,00*	*452*
27	***240***	*0,11*	*0,01*	*0,11*	*0,48*	*100*	*436*	*0,08*	*443*
26	***218***	*0,04*	*0,00*	*0,03*	*0,45*	*75*	*1125*	*0,00*	*510*
25	***214***	*3,33*	*0,51*	*18,87*	*0,67*	*567*	*20*	*0,03*	*427*
24	***207***	*0,31*	*0,01*	*0,62*	*0,66*	*200*	*213*	*0,02*	*439*
23	***204***	*0,03*	*0,00*	*0,02*	*0,19*	*67*	*633*	*0,00*	*443*
22	***200***	*0,07*	*0,01*	*0,07*	*0,48*	*100*	*686*	*0,13*	*440*
21	***167***	*0,05*	*0,00*	*0,03*	*0,33*	*60*	*660*	*0,00*	*499*
20	***161***	*0,52*	*0,06*	*2,63*	*0,26*	*506*	*50*	*0,02*	*431*
19	***120***	*0,81*	*0,14*	*5,22*	*0,21*	*644*	*26*	*0,03*	*431*
18	***118***	*0,16*	*0,01*	*0,33*	*0,43*	*206*	*269*	*0,03*	*441*
17	***115***	*0,03*	*0,00*	*0,02*	*0,37*	*67*	*1233*	*0,00*	*514*
16	***113***	*0,03*	*0,00*	*0,02*	*0,15*	*67*	*500*	*0,00*	*472*
15	***100***	*0,07*	*0,01*	*0,04*	*0,33*	*57*	*471*	*0,20*	*435*
14	***91***	*0,05*	*0,01*	*0,05*	*0,31*	*100*	*620*	*0,17*	*437*
13	***86***	*0,03*	*0,00*	*0,03*	*0,27*	*100*	*900*	*0,00*	*457*
12	***84***	*0,1*	*0,01*	*0,07*	*0,33*	*70*	*330*	*0,13*	*441*
11	***81***	*0,04*	*0,00*	*0,03*	*0,17*	*75*	*425*	*0,00*	*443*
10	***75***	*0,07*	*0,01*	*0,05*	*0,10*	*71*	*143*	*0,17*	*435*
9	***69***	*0,03*	*0,00*	*0,03*	*0,26*	*100*	*867*	*0,00*	*488*
8	***66***	*0,03*	*0,00*	*0,02*	*0,27*	*67*	*900*	*0,00*	*490*
7	***62***	*0,09*	*0,00*	*0,05*	*0,31*	*56*	*344*	*0,00*	*439*
6	***41***	*0,03*	*0,01*	*0,04*	*0,30*	*133*	*1000*	*0,20*	*509*
5	***21***	*0,02*	*0,00*	*0,03*	*0,07*	*150*	*350*	*0,00*	*441*
4	***18***	*0,03*	*0,00*	*0,03*	*0,09*	*100*	*300*	*0,00*	*444*
3	***15***	*0,03*	*0,00*	*0,02*	*0,07*	*67*	*233*	*0,00*	*437*
2	***5***	*0,06*	*0,01*	*0,05*	*0,26*	*83*	*433*	*0,17*	*447*
1	***1***	*0,04*	*0,01*	*0,04*	*0,11*	*100*	*275*	*0,20*	*434*